E2Former: An Efficient and Equivariant Transformer with Linear-Scaling Tensor Products

Yunyang Li^{1†}, Lin Huang^{2† ‡*}, Zhihao Ding³, Chu Wang ⁴, Xinran Wei ^{5‡}, Han Yang⁶, Zun Wang^{7‡}, Chang Liu^{5‡}, Yu Shi^{5‡}, Peiran Jin ^{5‡}, Tao Oin^{5‡}, Mark Gerstein^{1*}, Jia Zhang^{2*‡}

¹Yale University, ²Ubiquant, ³PolyU, ⁴HUST, ⁵ZGC Academy, ⁶Microsoft Research, ⁷Shanghai AI Lab https://github.com/liyy2/E2Former

Abstract

Equivariant Graph Neural Networks (EGNNs) have demonstrated significant success in modeling microscale systems, including those in chemistry, biology and materials science. However, EGNNs face substantial computational challenges due to the high cost of constructing edge features via spherical tensor products, making them almost impractical for large-scale systems. To address this limitation, we introduce E2Former, an equivariant and efficient transformer architecture that incorporates a Wigner 6j convolution (Wigner 6j Conv). By shifting the computational burden from edges to nodes, Wigner 6j Conv reduces the complexity from $O(|\mathcal{E}|)$ to $O(|\mathcal{V}|)$ while preserving both the model's expressive power and rotational equivariance. We show that this approach achieves a 7x–30x speedup compared to conventional SO(3) convolutions. Furthermore, our empirical results demonstrate that the derived E2Former mitigates the computational challenges of existing approaches without compromising the ability to capture detailed geometric information. This development could suggest a promising direction for scalable molecular modeling.

1 Introduction

Molecular simulations underpin critical computational tasks across chemistry [31, 36, 38, 39], biology [9], and materials science [64], facilitating detailed exploration of microscopic processes. Although quantum mechanical approaches such as Density Functional Theory (DFT) provide highly accurate predictions [30, 37], their computational complexity scales poorly with system size [56], thus limiting practical applicability to small-scale problems. Machine Learning (ML) techniques have emerged as promising alternatives, balancing computational efficiency and accuracy [5, 4, 16]. ML-based models, particularly Equivariant Graph Neural Networks (EGNNs), significantly reduce simulation times, enabling molecular property predictions and dynamic simulations within practical computational budgets [53, 26, 25, 7, 23, 41]. EGNN architectures explicitly encode symmetry constraints—such as rotational and reflectional equivariances—through graph-based atomic representations. This symmetry-awareness leads to strong inductive biases and improved sample efficiency. EGNNs have evolved from rotationally invariant embedding methods like SchNet [53] to schemes incorporating bond and dihedral angles [26, 25], scalarization techniques [52, 63], and spherical tensor-product frameworks such as E(3) and SE(3)-Transformers [57, 28, 23, 41]. Recent refinements, including Gaunt Tensor Product [44] eSCN convolutions [47, 42], primarily focus on enhancing computational efficiency.

[†]Co-first authors.

[‡]Part of this work was completed while the authors were at Microsoft Research.

^{*}Corresponding authors. huang_6385@outlook.com, pi@gersteinlab.org, jialrs.z@gmail.com *Note: JZ and LH (Ubiquant) thank ScitiX for computing power and training infrastructure. MG is supported by the ALW professorship fund.

In this work, we specifically focus on spherical-equivariant EGNN architectures [57, 23, 41], which leverage spherical harmonics and Clebsch-Gordan tensor products. These models—commonly referred to as spherical EGNNs—have demonstrated state-of-the-art accuracy, especially for periodic systems where symmetry constraints are critical [59, 10]. By encoding higher-order geometric correlations through irreducible representations (irreps) with angular momentum L > 1, spherical EGNNs offer expressive, data-efficient models capable of capturing complex geometric interactions [57, 55]. Unfortunately, these gains come at a computational cost. The use of spherical tensor products for feature construction incurs complexity driven by two factors: (i) the number of tensor products required, which scales with the number of edges $|\mathcal{E}|$ in the molecular graph, and (ii) the computational cost of each tensor product, which grows with the angular momentum cutoff L. Together, these lead to runtime costs of $O(|\mathcal{E}|L^6)$ or $O(|\mathcal{E}|L^3)$ when implemented with the sparse eSCN convolution. This scaling presents a significant bottleneck, limiting the use of spherical EGNNs to small- or mediumscale systems, despite their improved performance in principle. While recent spherical-scalarization methods [52, 63, 2] offer efficient alternatives by bypassing tensor products, they sacrifice theoretical completeness [18]. Tensor-product formulations, in contrast, preserve the full space of equivariant functions between irreps. This trade-off motivates our effort to retain the expressive power of tensor products while eliminating their prohibitive complexity.

Here, we introduce the Wigner 6j convolution (Wigner 6j Conv, Figure 1), a spherical-equivariant method that uses Wigner 6j symbols [40, 45, 20], *provably* reducing tensor product complexity to $O(|\mathcal{V}|)$ while maintaining the *exact expressive power* and rotational equivariance.

Contributions. Our contributions can be summarized as follows: (1) We introduce the Wigner 6j convolution, a spherical-equivariant technique that reduces the computational complexity from $O(|\mathcal{E}|)$ to $O(|\mathcal{V}|)$, enabling the modeling of larger molecular systems without compromising the network's expressive power or symmetry properties. As shown in Figure 2(b), our model demonstrates better scaling behavior than the SO(3) convolution, achieving 7x to 30x speed-up given the sparsity of the molecular graph. (2) We propose E2Former, an equivariant and efficient Transformer architecture specifically designed for scalable molecular modeling. E2Former leverages the Wigner 6j convolution to maintain rotational equivariance while significantly enhancing computational efficiency. (3) Extensive experiments on benchmark datasets like OC20, OC22, and SPICE show that E2Former achieves competitive accuracy in predicting molecular energies and forces, while offering improved efficiency and scalability over existing spherical-equivariant methods. (4) Finally, we pre-trained E2Former on a large-scale dataset and evaluated its performance in molecular dynamics simulations, where it achieves high accuracy with faster speed, outperforming state-of-the-art empirical potential methods and EGNNs. These results suggest its potential to advance large-scale molecular simulations and to serve as a foundational model for machine learning force fields.

2 Background and Preliminaries

Notation. Throughout this paper, we use ℓ and m to denote angular momentum quantum numbers associated with spherical harmonics $Y_m^{(\ell)}$, where $\ell \geq 0$ and $-\ell \leq m \leq \ell$. All spherical harmonics are considered real-valued functions on \mathbb{R}^3 . Positions of nodes in \mathbb{R}^3 are represented as \mathbf{r} , while node-level irreducible features are denoted $\mathbf{h}_i \in \mathbb{R}^{s \times c}$, where s represents the spherical dimension and s the feature dimension per spherical component (i.e. number of channels). The operation $[...]^{(\ell)}$ is the *projection operation* which extracts only the ℓ -th order irreducible component from a representation or tensor product. Clebch-Gorden Tensor products of irreps are symbolized by \otimes (without any superscripts), and its Wigner 6j counterpart is denoted by \otimes^{6j} .

In this section, we establish the mathematical foundations necessary for constructing the Wigner-6*j* Convolution. These include real-space *solid spherical harmonics*, tensor products of irreducible representations (irreps), and Wigner 6*j recoupling* theory. We commence by defining the solid spherical harmonics in real basis, which is commonly used in modern ML applications:

Definition 2.1 (Solid Spherical Harmonics in Real Basis). Let $\mathbf{r}=(x,y,z)\in\mathbb{R}^3, r=\|\mathbf{r}\|=\sqrt{x^2+y^2+z^2}$, and (r,θ,ϕ) be the spherical coordinates with:

$$\theta = \arccos\left(\frac{z}{r}\right), \qquad \phi = \operatorname{atan2}(y, x).$$

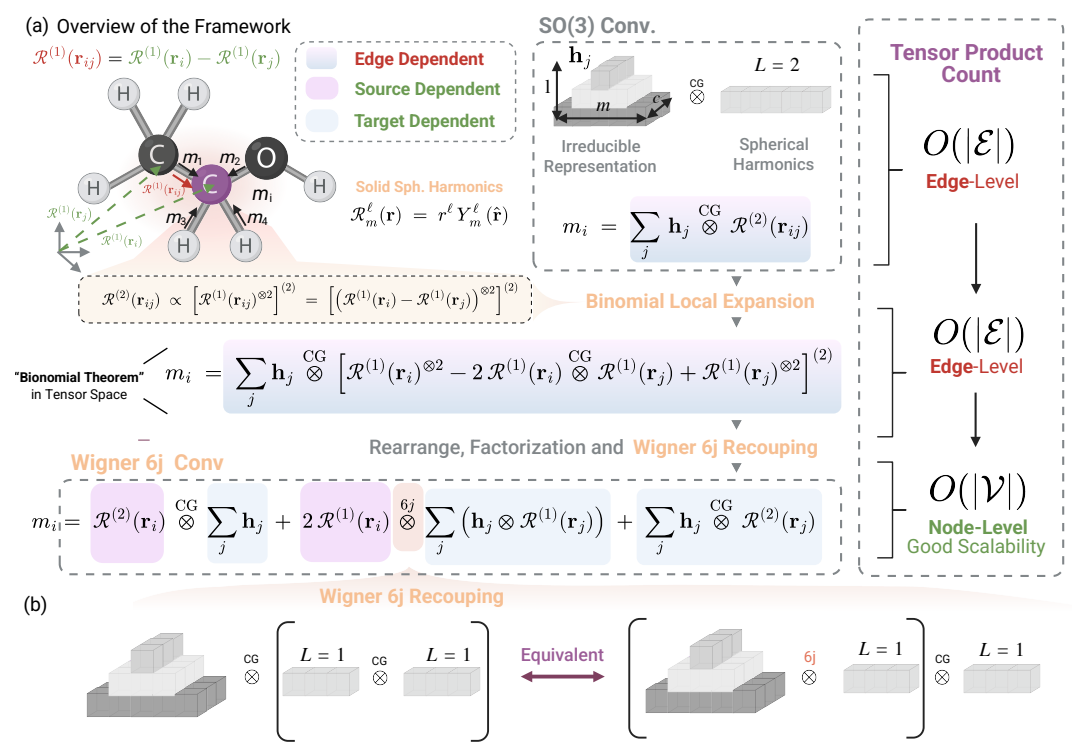


Figure 1: (a) Overview of the Proposed Approach. Rather than performing tensor products over edges by combining node features and distances, E2Former leverages two key concepts: binomial local expansion and Wigner 6j recoupling. The former represents edge directions in terms of node positions, while the latter reorders the sequence of tensor product operations. Together, the computational complexity of the tensor product is reduced from $O(|\mathcal{E}|)$ to $O(|\mathcal{V}|)$. \otimes denotes the Clebsch-Gorden tensor product, and \otimes^{6j} denotes the CG tensor product where each path is parameterized by a weight governed by the Wigner-6j coefficients. (b) Illustration of two equivalent ways to couple the tensor product of three representations: sequentially coupling two tensors before the third (left) or reordering the coupling sequence (right), with equivalence established via the Wigner 6j recoupling.

The (regular) solid spherical harmonics are homogeneous harmonic polynomials of degree ℓ defined by:

$$\mathcal{R}_m^{(\ell)}(\mathbf{r}) \ = \ r^\ell \, Y_m^{(\ell)}(\hat{\mathbf{r}}), \qquad \hat{\mathbf{r}} = \mathbf{r}/r, \quad \ell \ge 0, \ -\ell \le m \le \ell,$$

where $Y_m^{(\ell)}$ are real spherical harmonics on S^2 . Equivalently, in (r, θ, ϕ) ,

$$\mathcal{R}_{m}^{(\ell)}(r,\theta,\phi) = \begin{cases} k_{m}^{(\ell)} r^{\ell} P_{m}^{(\ell)}(\cos\theta) \cos(m\phi), & m > 0, \\ k_{0}^{(\ell)} r^{\ell} P_{0}^{(\ell)}(\cos\theta), & m = 0, \\ k_{|m|}^{(\ell)} r^{\ell} P_{|m|}^{(\ell)}(\cos\theta) \sin(|m|\phi), & m < 0, \end{cases}$$

with $P_{|m|}^{(\ell)}$ the associated Legendre polynomials and $k_m^{(\ell)}$ normalization constants (chosen per the convention used in this work). For example, in e3nn implementation, the real spherical harmonics for $\ell=2$ take the following form in Cartesian coordinates: $\mathcal{R}_{-2}^{(2)}(x,y,z)=xy,\mathcal{R}_{-1}^{(2)}(x,y,z)=yz,\mathcal{R}_{-2}^{(2)}(x,y,z)=xy,\mathcal{R}_{-2}^{(2)}(x,y,z)=yz,\mathcal{R}_{-2}^{(2)}(x,y,z)=x^2-y^2$. Under a rotation $g\in \mathrm{SO}(3)$, these functions transform according to: $\mathcal{R}_m^{(\ell)}(\mathbf{r})\mapsto\sum_{m'=-\ell}^{(\ell)}D_{m,m'}^{(\ell)}(g)\,\mathcal{R}_{m'}^{(\ell)}(\mathbf{r})$, where $D_{m,m'}^{(\ell)}(g)$ are the Wigner D-matrices. This transformation rule ensures that spherical harmonics of fixed degree ℓ transform properly under the action of $\mathrm{SO}(3)$. One useful property of solid spherical harmonics that will come in useful later is $\mathcal{R}^{(1)}(\mathbf{r}_{ij})=\mathcal{R}^{(1)}(\mathbf{r}_i)-\mathcal{R}^{(1)}(\mathbf{r}_j)$. It is also worth noting that this equality holds universally if and only if $\ell=1$.

Next, we introduce the behavior of irreducible representations (irreps). A key principle is that the tensor product of two irreps is generally reducible, meaning it decomposes into a direct sum of other

irreps. This decomposition mechanism is precisely what will allow us to relate the general irrep $\mathcal{R}^{(\ell)}(\cdot)$ back to $\mathcal{R}^{(1)}(\cdot)$.

Definition 2.2 (Tensor Products of Irreps). Let $U^{(\ell_1)}$ and $U^{(\ell_2)}$ be irreducible representations (irreps) of SO(3). Their tensor product $U^{(\ell_1)} \otimes U^{(\ell_2)}$ decomposes into a direct sum of irreps: $U^{(\ell_1)} \otimes U^{(\ell_2)} = \bigoplus_{\ell=|\ell_1-\ell_2|}^{\ell_1+\ell_2} U^{(\ell)}$. The decomposition is governed by the **Clebsch–Gordan coefficients**. Specifically, the tensor product, projected onto a specific irreducible component $U^{(\ell_3)}$, is denoted as:

$$\left[U^{(\ell_1)} \otimes U^{(\ell_2)}\right]^{(\ell_3)} = \sum_{\ell_1 m_1, \ell_2 m_2} C_{\ell_1 m_1, \ell_2 m_2}^{\ell_3 m_3} U_{m_1}^{(\ell_1)} U_{m_2}^{(\ell_2)}. \tag{2.1}$$

Commutativity of the Clebsch–Gordan Tensor Product. The tensor product of two irreducible representations (irreps) $U^{(a)}$ and $U^{(b)}$ of $\mathrm{SO}(3)$ is not strictly commutative as a bilinear operation on vector spaces: $U^{(a)}\otimes U^{(b)}$ is not identical to $U^{(b)}\otimes U^{(a)}$. Nonetheless, this operation is *effectively* commutative at the level of irreducible decompositions. Interchanging the order of the factors does not change the set of irreps that appear, although it permutes the corresponding CG coefficients. In particular, we have:

$$U^{(a)} \otimes U^{(b)} \cong U^{(b)} \otimes U^{(a)} \cong \bigoplus_{j=|a-b|}^{a+b} U^{(j)}. \tag{2.2}$$

Associativity of the Clebsch–Gordan Tensor Product. For irreducible representations (irreps) of SO(3), the tensor product is associative up to a canonical isomorphism. Specifically, for any three irreps $U^{(a)}$, $U^{(b)}$, and $U^{(c)}$, the following holds:

$$(U^{(a)} \otimes U^{(b)}) \otimes U^{(c)} \cong U^{(a)} \otimes (U^{(b)} \otimes U^{(c)}).$$

While the set of resulting irreps is independent of the association order, the CG coefficients that appear in the decomposition do depend on the chosen coupling scheme. Transitions between different coupling orders are governed by Wigner 6j symbols, which express changes of basis without modifying the underlying irreducible content.

Definition 2.3 (Wigner 6j Symbol). For three irreps $U^{(a)}$, $U^{(b)}$, and $U^{(c)}$ of SO(3), one can couple them either as $U^{(a)} \otimes (U^{(b)} \otimes U^{(c)})$ or as $(U^{(a)} \otimes U^{(b)}) \otimes U^{(c)}$. The Wigner 6j symbol $\begin{cases} a & b & d \\ c & \ell & j \end{cases}$ relates these two coupling schemes through the identity:

$$\left[U^{(a)} \otimes \left[U^{(b)} \otimes U^{(c)} \right]^{(j)} \right]^{(\ell)} = \sum_{d} (-1)^{a+b+c+d} \sqrt{(2d+1)(2j+1)} \begin{cases} a & b & d \\ c & \ell & j \end{cases} \left[U^{(a)} \otimes U^{(b)} \right]^{(d)} \otimes U^{(c)}.$$
(2.3)

To simplify notation, we abstract the recoupling process as follows:

$$U^{(a)} \otimes (U^{(b)} \otimes U^{(c)}) = (U^{(a)} \otimes U^{(b)}) \otimes^{6j} U^{(c)}, \tag{2.4}$$

where \otimes^{6j} denotes a CG tensor product accompanied by a re-indexing via Wigner 6j coefficients.

3 Wigner 6*j* Convolution

In this section, we introduce the SO(3)-Equivariant Node convolution and demonstrate how Wigner 6j recoupling facilitates an efficient node-wise computation.

Definition 3.1 (SO(3)-Equivariant Node Convolution). Let $\mathbf{h}_i \in \mathbb{R}^{s \times c}$ denote the irreducible feature tensor of node i, where s indexes the irreducible representation (irrep) type and c indexes the channels within each irrep. Let $\mathcal{R}^{(\ell)}(\mathbf{r}_{ij})$ denote the degree- ℓ spherical harmonic evaluated at the relative direction. The SO(3)-equivariant node convolution is via the CG tensor product between the source irreps and the spherical harmonics: $\mathbf{h}_i := \sum_{j \in \mathcal{N}(i)} \mathbf{h}_j \otimes \mathcal{R}^{(\ell)}(\mathbf{r}_{ij})$.

We clarify that our formulation of the SO(3) convolution employs $\mathcal{R}(\cdot)$ rather than $Y(\cdot)$. The two formulations are related through a normalization factor. To realize the $Y(\cdot)$ -based variant, this normalization factor can be absorbed into the attention coefficients, as detailed in Alg. 1.

Wigner 6j **convolution.** Given the SO(3) convolution, we aim to demonstrate that the operation admits a node-wise factorization via Wigner 6j symbols. In particular, we show that the SO(3) convolution can be expressed as:

$$\mathbf{h}_i = \sum_{j \in \mathcal{N}(i)} \underbrace{\left(\mathbf{h}_j \otimes \mathcal{R}^{(\ell)}(\mathbf{r}_{ij})\right)}_{\text{ij-dependent}} = \sum_{u=0}^{\ell} (-1)^{\ell-u} \binom{\ell}{u} \underbrace{\left(\underbrace{\mathcal{R}^{(u)}(\mathbf{r}_i)}_{\text{i-dependent}}\right)}_{\text{ij-dependent}} \otimes^{6j} \left(\sum_{j \in \mathcal{N}(i)} \underbrace{\left(\mathbf{h}_j \otimes \left(\mathcal{R}^{(\ell-u)}(\mathbf{r}_j)\right)\right)}_{\text{j-dependent}}\right).$$

The blue–boxed factors $\mathcal{R}^{(u)}(\vec{r_i})$ aggregate all node-i–specific terms, whereas the red–boxed factors \mathbf{h}_j , $\mathcal{R}^{(\ell-u)}(\vec{r_j})$ isolate the node-j contribution. This separation removes explicit edge dependencies, resulting in the number of tensor products in the network scaling with O(|V|). To build further intuition, we draw an analogy to factorization techniques in kernelized attention mechanisms [13], which achieve linear scaling by decoupling query-key interactions.

To establish this result, we introduce the concept of the *Binomial Local Expansion*. The expansion is based on the key insight that any term $\mathcal{R}^{(\ell)}(\cdot)$ of arbitrary order ℓ can be expressed through iterative tensor products of the first-order term, $\mathcal{R}^{(1)}(\cdot)$. This effectively reduces the problem to the first-order case, where we can apply the previously introduced relation $\mathcal{R}^{(1)}(\mathbf{r}_{ij}) = \mathcal{R}^{(1)}(\mathbf{r}_i) - \mathcal{R}^{(1)}(\mathbf{r}_j)$ to factor the edge-dependent expression into node-local terms.

Theorem 3.2 (Bionomial Local Expansion). Let $\ell = u \geq 1$. Every $\ell = u$ spherical harmonic $\mathcal{R}^{(l)}(\mathbf{r}_{ij})$ can be expressed as an irreducible subspace of the u-fold tensor product $(\mathcal{R}^{(1)}(\mathbf{r}_{ij}))^{\otimes u}$. When expanded in terms of node-local terms, this satisfies:

$$\mathcal{R}^{(\ell)}(\mathbf{r}_{ij}) = \sum_{u=0}^{\ell} (-1)^{\ell-u} \binom{\ell}{u} \left[\left(\mathcal{R}^{(u)}(\mathbf{r}_i) \right) \otimes \left(\mathcal{R}^{(\ell-u)}(\mathbf{r}_j) \right) \right]^{(\ell)},$$

Proof Sketch. This spherical harmonic $\mathcal{R}^{(\ell)}(\mathbf{r}_{ij})$ could be constructed by projecting the ℓ -fold tensor product of the first-order harmonic $\mathcal{R}^{(1)}(\mathbf{r}_{ij})$ onto the subspace transforming as the irreducible representation (irrep) ℓ of SO(3). Recall that the projection operator is denoted by $[...]^{(\ell)}$ and using the identity $\mathcal{R}^{(1)}(\mathbf{r}_{ij}) = \mathcal{R}^{(1)}(\mathbf{r}_i) - \mathcal{R}^{(1)}(\mathbf{r}_j)$, the objective could be rewritten as $\mathcal{R}^{(\ell)}(\mathbf{r}_{ij}) = [(\mathcal{R}^{(1)}(\mathbf{r}_i) - \mathcal{R}^{(1)}(\mathbf{r}_j))^{\otimes \ell}]^{(\ell)}$.

We begin by expanding the tensor power $(\mathcal{R}^{(1)}(\mathbf{r}_i) - \mathcal{R}^{(1)}(\mathbf{r}_j))^{\otimes \ell}$, which produces a sum of 2^ℓ tensor products. Each term corresponds to an ordered sequence $P \in \{i,j\}^\ell$, where each factor is either $\mathcal{R}^{(1)}(\mathbf{r}_i)$ or $\mathcal{R}^{(1)}(\mathbf{r}_j)$. Denote the corresponding tensor product as T_P . For example, if P = (i,j,i), then $T_P = \mathcal{R}^{(1)}(\mathbf{r}_i) \otimes \mathcal{R}^{(1)}(\mathbf{r}_j) \otimes \mathcal{R}^{(1)}(\mathbf{r}_i)$. Initially, each ordering $(*,*,*,\cdots,*)$ defines a distinct term. Later, we will show that the projection operator renders the result invariant to the ordering. We write the full expansion as: $(\mathcal{R}^{(1)}(\mathbf{r}_i) - \mathcal{R}^{(1)}(\mathbf{r}_j))^{\otimes \ell} = \sum_{u=0}^\ell (-1)^{\ell-u} \sum_{P \in \Pi_u} T_P$, where Π_u denotes the set of orderings containing exactly u factors of $\mathcal{R}^{(1)}(\mathbf{r}_i)$ and $\ell-u$ factors of $\mathcal{R}^{(1)}(\mathbf{r}_j)$. Applying the linear projection operator $[\ldots]^{(\ell)}$ to this sum distributes the operator yields $[(\mathcal{R}^{(1)}(\mathbf{r}_i) - \mathcal{R}^{(1)}(\mathbf{r}_j))^{\otimes \ell}]^{(\ell)} = \sum_{u=0}^\ell (-1)^{\ell-u} \sum_{P \in \Pi_u} [T_P]^{(\ell)}$.

The key insight comes from angular momentum coupling theory. Combining ℓ systems with angular momentum 1 yields components with total angular momentum ranging up to ℓ . The subspace associated with the *highest possible* angular momentum, $L=\ell$, is *unique* and corresponds to the *fully symmetric* combination of the individual factors. The projector $[...]^{(\ell)}$ isolates precisely this unique, symmetric component. As a result, the projected tensor $[T_P]^{(\ell)}$ remains identical for all orderings $P\in\Pi_u$, indicating that the projection depends solely on the multiplicities of the factors $\mathcal{R}^{(1)}(\mathbf{r}_i)$ and $\mathcal{R}^{(1)}(\mathbf{r}_j)$ in T_P , rather than their ordering. The inner sum over the $\binom{\ell}{u}$ identical projected terms simplifies. Let $T_{\text{rep}} = (\mathcal{R}^{(1)}(\mathbf{r}_i))^{\otimes u} \otimes (\mathcal{R}^{(1)}(\mathbf{r}_j))^{\otimes (\ell-u)}$ serve as a representative tensor product for the class Π_u . Then: $\sum_{P\in\Pi_u} [T_P]^{(\ell)} = |\Pi_u|[T_{\text{rep}}]^{(\ell)} = \binom{\ell}{u}[(\mathcal{R}^{(1)}(\mathbf{r}_i))^{\otimes u} \otimes (\mathcal{R}^{(1)}(\mathbf{r}_j))^{\otimes (\ell-u)}]^{(\ell)}$.

Substituting this simplification back into the expression for the projected tensor power yields: $[(\mathcal{R}^{(1)}(\mathbf{r}_i)-\mathcal{R}^{(1)}(\mathbf{r}_j))^{\otimes \ell}]^{(\ell)} = \sum_{u=0}^{\ell} (-1)^{\ell-u} \binom{\ell}{u} [(\mathcal{R}^{(1)}(\mathbf{r}_i))^{\otimes u} \otimes (\mathcal{R}^{(1)}(\mathbf{r}_j))^{\otimes (\ell-u)}]^{(\ell)}.$

Theorem 3.3 (Node-Based Factorization via Wigner 6j). SO(3) convolutions admit a factorization that separates the dependence on the central node i from the aggregation over neighbors j, yielding the form:

$$\sum_{j \in \mathcal{N}(i)} \mathbf{h}_j \otimes \mathcal{R}_m^{(\ell)}(\mathbf{r}_{ij}) = \sum_{u=0}^{\ell} (-1)^{\ell-u} \binom{\ell}{u} \left(\mathcal{R}^{(u)}(\mathbf{r}_i) \right) \otimes^{6j} \left(\sum_{j \in \mathcal{N}(i)} \mathbf{h}_j \otimes \left(\mathcal{R}^{(\ell-u)}(\mathbf{r}_j) \right) \right),$$

where \otimes^{6j} denotes a CG tensor product where the path weight is parameterized by the corresponding Wigner 6j coefficients.

Proof Sketch. We begin by substituting the spherical harmonic $\mathcal{R}_m^{(\ell)}(\mathbf{r}_{ij})$ using the binomial local expansion from into the original SO(3)-equivariant convolution expression, we obtain:

$$\sum_{j \in \mathcal{N}(i)} \mathbf{h}_j \otimes \sum_{u=0}^{\ell} (-1)^{\ell-u} \binom{\ell}{u} \left[\mathcal{R}^{(u)}(\mathbf{r}_i) \otimes \mathcal{R}^{(\ell-u)}(\mathbf{r}_j) \right]^{(\ell)}. \tag{3.1}$$

By linearity of the tensor product, this expression becomes:

$$\sum_{u=0}^{\ell} (-1)^{\ell-u} \binom{\ell}{u} \sum_{j \in \mathcal{N}(i)} \left(\mathbf{h}_j \otimes \left[\mathcal{R}^{(u)}(\mathbf{r}_i) \otimes \mathcal{R}^{(\ell-u)}(\mathbf{r}_j) \right]^{(\ell)} \right). \tag{3.2}$$

To reorganize this expression in terms of node-dependent features, we apply Wigner 6j recoupling. Letting $A = \mathbf{h}_j$, $B = \mathcal{R}^{(\ell-u)}(\mathbf{r}_j)$, $C = \mathcal{R}^{(u)}(\mathbf{r}_i)$, The recoupling identity states: $A \otimes (B \otimes C) = (A \otimes B) \otimes^{6j} C$. Since CG tensor products commute effectively, we can swap B and C before applying recoupling. This gives:

$$\mathbf{h}_{j} \otimes \left(\mathcal{R}^{(u)}(\mathbf{r}_{i}) \otimes \mathcal{R}^{(\ell-u)}(\mathbf{r}_{j}) \right) = \left(\mathbf{h}_{j} \otimes \mathcal{R}^{(\ell-u)}(\mathbf{r}_{j}) \right) \otimes^{6j} \mathcal{R}^{(u)}(\mathbf{r}_{i}). \tag{3.3}$$

Applying this recoupling within the sum, we arrive at the factorized form as claimed. Note that it is safe to apply the recoupling within a projection operator. This constraint can be implemented by fixing one of the intermediate coupling indices in the Wigner 6j symbol to ℓ .

We now formalize the key properties of the resulting Wigner 6j convolution. These results are stated in the following lemmas. Proofs are provided in Appendix E and Appendix F, respectively.

Lemma 3.4 (Equivariance of Wigner 6*j* Convolution). The Wigner 6*j* convolution operator (denoted as F), is equivariant under the Euclidean group SE(3). That is, for any rigid transformation $g \in SE(3)$, the output satisfies $\mathcal{F}[g \cdot f] = D(g) \cdot \mathcal{F}[f]$.

Lemma 3.5 (Time Complexity of Wigner 6j Convolution). The time complexity of Wigner 6j convolution is $O((L^6C + C^2L^2)|\mathcal{V}|)$, where L is the degree cutoff and C is the number of channels.

Model Architecture. Based on these, we propose E2Former, a modular architecture that alternates between E2Attention and feed-forward layers (Appendix Fig. 5(a); additional architectural details provided in the Appendix H). At its core lies a convolution layer based on the Wigner 6j convolution, which serves as a backend kernel to efficiently capture rotational symmetries. We highlight two key design considerations underlying E2Former. First, we observe that the attention computation constitutes only a small fraction of the overall runtime in an attention-based SO(3) convolution (Figure 2 (a)). Leveraging this, we integrate the attention mechanism directly into the Wigner 6j convolution (Algorithm 1). As a result, while the resulting model is not strictly linear, the number of tensor product operations scales linearly with input size, enabling efficient computation. Second, E2Former is not defined solely by its use of Wigner 6j convolutions. Rather, it represents a broader architectural principle that combines symmetry-aware design with practical engineering. The efficiency gains afforded by the Wigner 6j kernel allow us to reallocate the computational budget toward increased expressivity—e.g., by incorporating deeper layers, wider hidden dimensions, more attention heads, and MACE higher-order interactions [6]. This trade-off between symmetry-driven modeling and architectural scalability is central to the design philosophy of E2Former.

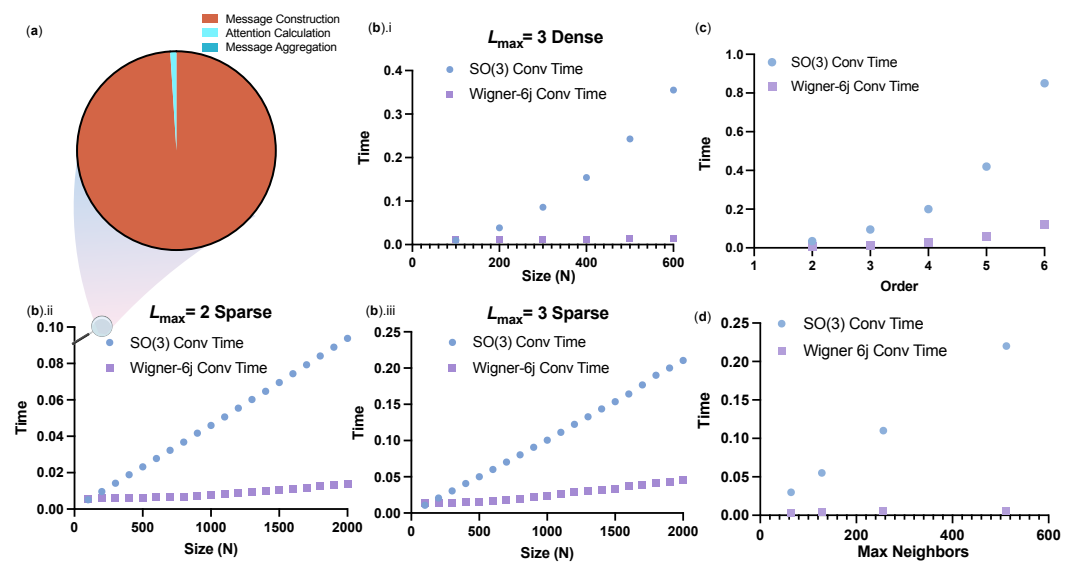


Figure 2: (a) Breaking down the runtime of attention-based SO(3) convolutions shows that message construction is the slowest step. Calculating attention and combining messages take much less time. (b) We compared the runtime of our Wigner 6j convolution (purple squares) against the standard SO(3) convolution (blue circles). Our method was consistently faster across different graph sizes (N), maximum angular momenta (L_{\max}) , and sparsity levels (dense vs. sparse, see subplots b.i-iii). Full experimental details are in Sec. 4.1. (c) Runtime on 1000-node graphs as a function of angular momentum cutoff L (up to $L_{\max}=6$). (d) Runtime on 1000-node graphs with fixed $L_{\max}=3$, varying the maximum number of neighbors from 64 to 512. In (b-d), both methods yield identical outputs.

4 Results

4.1 Scaling Analysis of Wigner 6i Conv and SO(3) Conv

Here, we compare the runtime of Wigner 6j convolution (purple squares) and $\mathrm{SO}(3)$ convolution (blue circles). The two implementations are mathematically equivalent and, by construction, produce identical outputs given the same molecular graphs. Specifically, we compare different graph sizes N, maximum angular momenta L_{max} , and connectivity patterns. For dense graphs, defined as graphs where every node is connected to all other nodes, at $L_{\mathrm{max}}=3$ (Fig. 2 (b.i)), the quadratic scaling of $\mathrm{SO}(3)$ convolution introduces a noticeable performance gap. Additionally, for sparse graphs, defined here as graphs with k-nearest neighbor connectivity (k=32), at $L_{\mathrm{max}}=2$ and $L_{\mathrm{max}}=3$ (Figs. 2 (b.ii) and (b.iii)), Wigner 6j convolution scales consistently better than the $\mathrm{SO}(3)$ convolution. Fig. 2c further shows the impact of increasing the angular momentum cutoff up to $L_{\mathrm{max}}=6$ on 1000-node graphs, where our method consistently achieves approximately a $7\times$ speed-up over the baseline. Finally, Fig. 2d demonstrates that as the number of neighbors per node increases from 64 to 512 (with $L_{\mathrm{max}}=3$), the speed-up from Wigner 6j convolution becomes even more pronounced.

4.2 E2Former Results

We evaluate E2Former which heavily utilizes the Wigner 6j convolution on three standard benchmarks—two catalysis datasets (OC20, OC22) and a molecular conformer dataset (SPICE)—and find that it achieves strong accuracy while maintaining computational efficiency.

4.2.1 Performance on the OC20 Dataset

Dataset Description. The OC20 dataset [10] comprises 1.2 million DFT relaxations computed using the revised Perdew-Burke-Ernzerhof (RPBE) functional [29]. Each system, averaging 73 atoms, represents an adsorbate molecule on a catalyst surface and is designed for the Structure-to-Energy-and-Forces (S2EF) task. This task involves predicting the system's energy and per-atom forces, with performance evaluated based on the mean absolute error (MAE) of these predictions. Following

[27, 41], we use the **2M** subset for training, and evaluate on the *validation split*. This choice also reflects practical computational constraints, as training on the full dataset requires significant time and resources. All reported results are taken directly from previous publications [27, 41]. We compare two model variants: the 33M-parameter version and the 67M-parameter version. A summary of the results is presented in Table 1. E2Former demonstrates strong performance across all model sizes, with 67M variant achieving results comparable to state-of-the-art methods. Notably, the Small variant (33M parameters) maintains competitive accuracy while offering significant computational advantages.

Table 1: Performance on the OC20-2M dataset. Results are reported in Energy (meV) and Force (meV/Å) mean absolute error (MAE). E2Former achieves competitive accuracy and computational efficiency. Approximate training GPU hours are measured on 32G NVIDIA V100 GPUs. The best results are bolded and the second best are highlighted with underline.

Model	# Params (M)	Training GPU Hours	Inference Speed (samples/sec)	Validation		
				Energy MAE (meV)	Force MAE (meV/Å)	
GemNet-dT	31	900	50	358	29.50	
GemNet-OC	38	1500	38	286	25.70	
SCN	126	3000	5	279	21.90	
eSCN	51	2200	19	283	<u>20.50</u>	
EquiformerV2	85	1800	19	285	20.46	
E2Former 33M	33	800	62	<u>275</u>	21.90	
E2Former 67M	67	1500	34	270	<u>20.50</u>	

4.2.2 Performance on the OC22 Dataset

The OC22 dataset [59] is specifically designed for studying oxide electrocatalysis. In contrast to OC20, OC22 features DFT total energies, which could serve as a general and versatile DFT surrogate, enabling investigations beyond adsorption energies. We train on the OC22 S2EF-Total task and measure energy and force MAE on the S2EF-Total validation splits. Table 2 summarizes our results on the OC22 S2EF task. E2Former achieves competitive energy and force MAEs while enabling rapid training and inference. Notably, it converges in just 1,500 GPU hours—only one-third of the runtime required by the SOTA model.

Table 2: Performance on the OC22 S2EF task. Results are reported for Energy MAE (meV) and Force MAE (meV/Å) under In Distribution (ID) and Out-Of-Distribution (OOD) splits. Approximate training GPU hours are measured on 32G NVIDIA V100 GPUs. The best results are bolded and the second best are highlighted with underline.

Model	# Params (M)	Training GPU Hours	Energy MAE (meV)		Force M	AE (meV/Å)
			ID	OOD	ID	OOD
GemNet-OC	39	-	545	1011	30.00	40.00
EquiformerV2	122	4500	433	629	22.88	30.70
E2Former 67M	67	1500	<u>491</u>	<u>724</u>	<u>25.98</u>	<u>36.45</u>

4.2.3 Performance on the SPICE Dataset

The SPICE dataset [19] comprises small organic molecules and encompasses a diverse array of chemical species with neutral formal charges. The geometries were generated through molecular dynamics simulations using classical force fields, followed by the sampling of various conformations. High-fidelity labeling was achieved at the $\omega B97M-D3(BJ)/def2-TZVPPD$ level of calculations. This dataset includes configurations of up to 50 atoms. It was further augmented with larger molecules, ranging from 50 to 90 atoms, derived from the QMugs dataset [32], as well as water clusters obtained from simulations of liquid water. Approximately 85% of the SPICE dataset was used for model training, while 15% was allocated for model testing. We evaluate E2Former 33M on the SPICE dataset and a summary of the results is provided in Table 3.

Table 3: Performance comparison on the SPICE dataset with actual training time and dataset sizes. Results are reported in Energy (E, meV/atom) and Force (F, meV/Å) MAE. Approximate training GPU hours are measured on 80G NVIDIA A100 GPUs.

Dataset Name (Size)	Training Time	PubCh	em (33884)	Monor	ners (889)	Dimer	s (13896)	Dipept	ides (1025)	Solvated	lAminoAcids (52)	Wate	er (84)	Qmug	gs (144)	A	All
	(gpu hours)	E	F	E	F	E	F	E	F	E	F	E	F	E	F	E	F
MACE Small	168	1.41	35.68	1.04	17.63	0.98	16.31	0.84	25.07	1.60	38.56	1.67	28.53	1.03	41.45	1.27	29.76
MACE Medium	240	0.91	20.57	0.63	9.36	0.58	9.02	0.52	14.27	1.21	23.26	0.76	15.27	0.69	23.58	0.80	17.03
MACE Large	336	0.88	14.75	0.59	6.58	0.54	6.62	0.42	10.19	0.98	19.43	0.83	13.57	0.45	16.93	0.77	12.26
E2Former 33M	70	0.67	8.9	0.49	7.1	0.43	4.01	0.51	5.63	1.1	19.2	0.96	13.52	0.65	10.2	0.60	7.46

E2Former achieved state-of-the-art performance in most subsets, particularly in datasets with ample data, such as PubChem and DEShaw370-Dimers. Furthermore, compared to the MACE-Large model, E2Former achieves approximately a *fivefold* increase in training speed, thereby further validating its efficiency.

4.3 Meomory and Efficiency Scaling

To further probe efficiency, we evaluated computational performance in an even more extreme case: system scale. We benchmarked E2Former against MACE-Large and EquiformerV2 on systems containing up to 6,400 atoms (Table 4). E2Former consistently achieved the highest throughput, with its performance advantage becoming clearer as system size increased. At 3,200 atoms, E2Former processes data nearly three times faster than MACE-Large. Crucially, E2Former was the only model capable of handling simulations at the 6,400-atom scale, a size at which both MACE-Large and EquiformerV2 failed.

Table 4: Comparison of memory cost and efficiency on large-scale systems with up to 6,400 atoms.

Atom Number	I I	Memory Cost (GB)	-	Training Efficiency (Samples/Second)				
	Equiformer V2-22M	MACE-Large-33M	E2Former-33M	Equiformer V2-22M	MACE-Large-33M	E2Former-33M		
200	14.2	6	3.9	1.81	5.1	4.5		
400	26.7	10.7	7.6	1.27	2.91	4.2		
800	53	23	16	0.68	1.61	2.36		
1600	-	38	20	0.83	0.81	2.46		
3200	-	74	40	-	0.41	1.2		
6400	-	-	80	-	-	0.59		

5 Molecular Dynamics Simulation

In this section, we demonstrate the practical utility of E2Former in molecular dynamics simulations. While machine learning methods are extensively used to predict molecular and material properties, accurately simulating the behavior of systems over extended time periods remains a significant challenge. This task requires not only precise predictions at each time step but also long-term stability and performance comparable to established methods such as DFT and empirical potential models.

We began by pretraining E2Former on a large inhouse dataset derived from DeShaw (2M) [15] and GEMS [60] (2.7M), constituting a *foundational model* on machine-learning force field.

5.1 Small-scale Amino Acid Systems

To evaluate the model, we first performed an NVT $(T=300\,\mathrm{K})$ simulation of an amino acid wrapped by water molecules (The structure is shown in Fig. 4(a)), totaling 253 atoms. This evaluation was conducted on a system equipped with a single NVIDIA A100 GPU

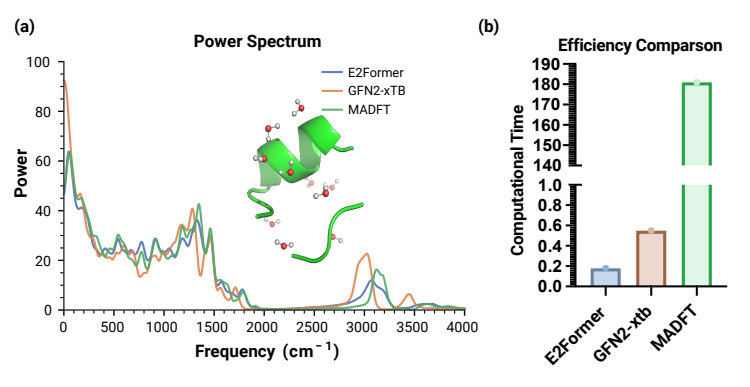


Figure 3: (a) Power spectra comparison across computational methods: E2Former (blue), GFN2-xTB (orange), and MADFT (green). The graph corresponds to a simulation at NVT ensemble, temperature $T=300\,\mathrm{K}$, with a time step of 1 fs. A structural overlay of the simulated system is displayed for context. (b) Efficiency comparison showing computational time for E2Former, GFN2-xtb, and MADFT. E2Former demonstrates the lowest computational time. The y-axis denotes the computation time for a single frame.

and an AMD EPYC 7V13 24-core CPU. Over the course of 10,000 simulation time steps (1fs per step), we compared the trajectory 's power spectrum obtained from E2Former, CUDA-accelerated DFT [34]- namely, the MADFT software and state-of-the-art empirical potential methods GFN2-xTB [3]. Fig. 4(a) illustrates the results. The evaluation demonstrates that E2Former exhibits long-term stability in molecular simulations. The power spectrum shows that E2Former predictions align closely with those of the DFT baseline. In contrast, empirical method shows significant devia-

tions in high-frequency regions, particularly near 3,000 and 3,500 frequencies. These high-frequency components are critical as they provide insights into bond vibrations [14] and molecular stability [12], underscoring the ability of E2Former to effectively extrapolate across the molecular potential energy surface. To assess computational efficiency, we compare runtime across methods, which is depicted in Fig. 4(b). E2Former achieves a computational speed approximately 1,000 times faster than DFT, and around 2 times faster than GFN2-xTB.

5.2 Large-Scale 6000-atom Water Cluster

To evaluate accuracy and efficiency at larger scales, we tested our model on a 6,000-atom water cluster by analyzing atomic vibration patterns. E2Former closely reproduced the reference DFT results, accurately capturing key spectral features: low-frequency modes (below 1000 cm⁻¹), the H–O–H bending mode (1650 cm⁻¹), and O–H stretching vibrations. In contrast, MACE-Large exhibited larger deviations, particularly for high-frequency stretching modes. We further validated our approach on a more complex system—a Chignolin peptide solvated in water (approximately 2,000 atoms, Fig 6)—successfully optimizing its structure

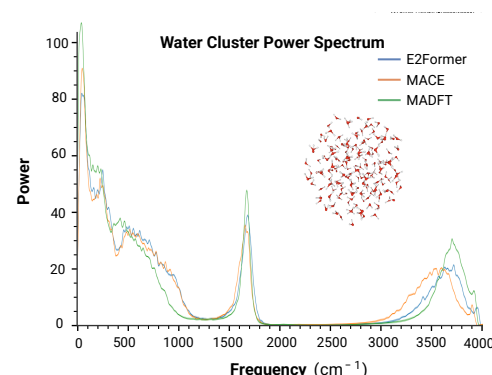


Figure 4: Power spectra comparison across computational methods: E2Former (blue), MACE (orange), and MADFT (green).

while maintaining high force prediction accuracy (0.484 kcal/mol/Å error).

6 Related Work

Invariant GNNs. Invariant geometric GNNs have driven state-of-the-art performance in predicting molecular and crystalline properties [53, 50, 11, 26, 43, 25, 62, 48] and have been instrumental in advancing protein structure prediction [35].

Cartesian Equivariant GNNs. Building on invariance, Cartesian equivariant GNNs explicitly model transformations in \mathbb{R}^3 , offering greater flexibility. These models have shown strong empirical results in similar domains [33, 51, 17, 54, 2] and have recently evolved to include Cartesian equivariant transformer layers [22].

Spherical Equivariant GNNs. Complementing Cartesian approaches, spherical equivariant GNNs leverage spherical tensors to naturally handle rotational symmetries, relying on the representation theory of SO(3). Recent advancements include SO(3)- and SE(3)-equivariant transformer layers [23, 41], efficient interatomic potential calculations [7, 6, 46], and optimizations that reduce convolutions in SO(3) to SO(2) [47]. These improvements have enabled strong performance in diverse applications, including geometry, physics, and chemistry [57], dynamic molecular modeling [1], and fluid mechanical modeling [58].

7 Conclusion and Future Work

We introduced E2Former, an efficient and scalable Transformer architecture for molecular modeling. By leveraging the Wigner 6j convolution, E2Former shifts computation from edges to nodes, reducing complexity from $O(|\mathcal{E}|)$ to $O(|\mathcal{V}|)$ while maintaining rotational equivariance and expressive power. E2Former demonstrated competitive performance across OC20, OC22, and SPICE benchmarks with significantly improved computational efficiency. Its scalability makes it suited for large-scale applications in biology, drug discovery, and materials science.

Future work could focus on optimizing E2Former for hardware accelerators and integrating kernelized Euclidean attention [21]. Combining Wigner-6j Conv with SO(2) convolution could further bolster the model's efficiency. Scaling to the real-world all-atom protein systems will also be investigated.

References

- [1] Brandon Anderson, Truong Son Hy, and Risi Kondor. Cormorant: Covariant molecular neural networks. *Advances in neural information processing systems*, 32, 2019.
- [2] Sarp Aykent and Tian Xia. GotenNet: Rethinking Efficient 3D Equivariant Graph Neural Networks. In *The Thirteenth International Conference on Learning Representations*, 2025.
- [3] Christoph Bannwarth, Sebastian Ehlert, and Stefan Grimme. Gfn2-xtb—an accurate and broadly parametrized self-consistent tight-binding quantum chemical method with multipole electrostatics and density-dependent dispersion contributions. *Journal of chemical theory and computation*, 15(3):1652–1671, 2019.
- [4] Albert P Bartók, Risi Kondor, and Gábor Csányi. On representing chemical environments. *Physical Review B—Condensed Matter and Materials Physics*, 87(18):184115, 2013.
- [5] Albert P Bartók, Mike C Payne, Risi Kondor, and Gábor Csányi. Gaussian approximation potentials: The accuracy of quantum mechanics, without the electrons. *Physical review letters*, 104(13):136403, 2010.
- [6] Ilyes Batatia, David Peter Kovacs, Gregor N. C. Simm, Christoph Ortner, and Gabor Csanyi. MACE: Higher order equivariant message passing neural networks for fast and accurate force fields. In Alice H. Oh, Alekh Agarwal, Danielle Belgrave, and Kyunghyun Cho, editors, Advances in Neural Information Processing Systems, 2022.
- [7] Simon Batzner, Albert Musaelian, Lixin Sun, Mario Geiger, Jonathan P Mailoa, Mordechai Kornbluth, Nicola Molinari, Tess E Smidt, and Boris Kozinsky. E(3)-equivariant graph neural networks for data-efficient and accurate interatomic potentials. *Nature communications*, 13(1):2453, 2022.
- [8] Lawrence C Biedenharn, James D Louck, and Peter A Carruthers. *Angular momentum in quantum physics: theory and application*. 1984.
- [9] Troy Cellmer, Marco Buscaglia, Eric R Henry, James Hofrichter, and William A Eaton. Making connections between ultrafast protein folding kinetics and molecular dynamics simulations. *Proceedings of the National Academy of Sciences*, 108(15):6103–6108, 2011.
- [10] Lowik Chanussot, Abhishek Das, Siddharth Goyal, Thibaut Lavril, Muhammed Shuaibi, Morgane Riviere, Kevin Tran, Javier Heras-Domingo, Caleb Ho, Weihua Hu, et al. Open catalyst 2020 (oc20) dataset and community challenges. *Acs Catalysis*, 11(10):6059–6072, 2021.
- [11] Chi Chen, Weike Ye, Yunxing Zuo, Chen Zheng, and Shyue Ping Ong. Graph networks as a universal machine learning framework for molecules and crystals. *Chemistry of Materials*, 31(9):3564–3572, 2019.
- [12] Choon-Peng Chng, Annette Dowd, Adam Mechler, and K Jimmy Hsia. Molecular dynamics simulations reliably identify vibrational modes in far-ir spectra of phospholipids. *Physical Chemistry Chemical Physics*, 2024.
- [13] Krzysztof Choromanski, Valerii Likhosherstov, David Dohan, Xingyou Song, Andreea Gane, Tamas Sarlos, Peter Hawkins, Jared Davis, Afroz Mohiuddin, Lukasz Kaiser, et al. Rethinking attention with performers. *arXiv preprint arXiv:2009.14794*, 2020.
- [14] Edward Ditler and Sandra Luber. Vibrational spectroscopy by means of first-principles molecular dynamics simulations. *Wiley Interdisciplinary Reviews: Computational Molecular Science*, 12(5):e1605, 2022.
- [15] Alexander G Donchev, Andrew G Taube, Elizabeth Decolvenaere, Cory Hargus, Robert T McGibbon, Ka-Hei Law, Brent A Gregersen, Je-Luen Li, Kim Palmo, Karthik Siva, et al. Quantum chemical benchmark databases of gold-standard dimer interaction energies. *Scientific data*, 8(1):55, 2021.
- [16] Ralf Drautz. Atomic cluster expansion for accurate and transferable interatomic potentials. *Physical Review B*, 99(1):014104, 2019.

- [17] Weitao Du, He Zhang, Yuanqi Du, Qi Meng, Wei Chen, Nanning Zheng, Bin Shao, and Tie-Yan Liu. Se (3) equivariant graph neural networks with complete local frames. In *International Conference on Machine Learning*, pages 5583–5608. PMLR, 2022.
- [18] Nadav Dym and Haggai Maron. On the universality of rotation equivariant point cloud networks. In *International Conference on Learning Representations*.
- [19] Peter Eastman, Pavan Kumar Behara, David L Dotson, Raimondas Galvelis, John E Herr, Josh T Horton, Yuezhi Mao, John D Chodera, Benjamin P Pritchard, Yuanqing Wang, et al. Spice, a dataset of drug-like molecules and peptides for training machine learning potentials. *Scientific Data*, 10(1):11, 2023.
- [20] Alan Robert Edmonds. *Angular momentum in quantum mechanics*, volume 4. Princeton university press, 1996.
- [21] J Thorben Frank, Stefan Chmiela, Klaus-Robert Müller, and Oliver T Unke. Euclidean fast attention: Machine learning global atomic representations at linear cost. *arXiv preprint arXiv:2412.08541*, 2024.
- [22] J Thorben Frank, Oliver T Unke, and Klaus-Robert Müller. So3krates-self-attention for higher-order geometric interactions on arbitrary length-scales. arXiv preprint arXiv:2205.14276, 2022.
- [23] Fabian Fuchs, Daniel Worrall, Volker Fischer, and Max Welling. Se (3)-transformers: 3d roto-translation equivariant attention networks. Advances in Neural Information Processing Systems, 33:1970–1981, 2020.
- [24] William Fulton and Joe Harris. *Representation theory: a first course*, volume 129. Springer Science & Business Media, 2013.
- [25] Johannes Gasteiger, Florian Becker, and Stephan Günnemann. Gemnet: Universal directional graph neural networks for molecules. *Advances in Neural Information Processing Systems*, 34:6790–6802, 2021.
- [26] Johannes Gasteiger, Janek Groß, and Stephan Günnemann. Directional message passing for molecular graphs. *arXiv preprint arXiv:2003.03123*, 2020.
- [27] Johannes Gasteiger, Muhammed Shuaibi, Anuroop Sriram, Stephan Günnemann, Zachary Ulissi, C Lawrence Zitnick, and Abhishek Das. Gemnet-oc: developing graph neural networks for large and diverse molecular simulation datasets. *arXiv preprint arXiv:2204.02782*, 2022.
- [28] Mario Geiger, Tess Smidt, Alby M., Benjamin Kurt Miller, Wouter Boomsma, Bradley Dice, Kostiantyn Lapchevskyi, Maurice Weiler, Michał Tyszkiewicz, Simon Batzner, Dylan Madisetti, Martin Uhrin, Jes Frellsen, Nuri Jung, Sophia Sanborn, Mingjian Wen, Josh Rackers, Marcel Rød, and Michael Bailey. Euclidean neural networks: e3nn, April 2022.
- [29] BHLB Hammer, Lars Bruno Hansen, and Jens Kehlet Nørskov. Improved adsorption energetics within density-functional theory using revised perdew-burke-ernzerhof functionals. *Physical review B*, 59(11):7413, 1999.
- [30] Pierre Hohenberg and Walter Kohn. Inhomogeneous electron gas. *Physical review*, 136(3B):B864, 1964.
- [31] Gyeong S Hwang, Haley M Stowe, Eunsu Paek, and Dhivya Manogaran. Reaction mechanisms of aqueous monoethanolamine with carbon dioxide: a combined quantum chemical and molecular dynamics study. *Physical Chemistry Chemical Physics*, 17(2):831–839, 2015.
- [32] Clemens Isert, Kenneth Atz, José Jiménez-Luna, and Gisbert Schneider. Qmugs, quantum mechanical properties of drug-like molecules. *Scientific Data*, 9(1):273, 2022.
- [33] Bowen Jing, Stephan Eismann, Patricia Suriana, Raphael John Lamarre Townshend, and Ron Dror. Learning from protein structure with geometric vector perceptrons. In *International Conference on Learning Representations*, 2020.

- [34] Fusong Ju, Xinran Wei, Lin Huang, Andrew J Jenkins, Leo Xia, Jia Zhang, Jianwei Zhu, Han Yang, Bin Shao, Peggy Dai, et al. Acceleration without disruption: Dft software as a service. *Journal of Chemical Theory and Computation*, 20(24):10838–10851, 2024.
- [35] John Jumper, Richard Evans, Alexander Pritzel, Tim Green, Michael Figurnov, Olaf Ronneberger, Kathryn Tunyasuvunakool, Russ Bates, Augustin Žídek, Anna Potapenko, et al. Highly accurate protein structure prediction with alphafold. *Nature*, 596(7873):583–589, 2021.
- [36] Ferenc Karsai, Manuel Engel, Espen Flage-Larsen, and Georg Kresse. Electron-phonon coupling in semiconductors within the gw approximation. New Journal of Physics, 20(12):123008, 2018.
- [37] Walter Kohn and Lu Jeu Sham. Self-consistent equations including exchange and correlation effects. *Physical review*, 140(4A):A1133, 1965.
- [38] Arpan Kundu, Marco Govoni, Han Yang, Michele Ceriotti, Francois Gygi, and Giulia Galli. Quantum vibronic effects on the electronic properties of solid and molecular carbon. *Physical Review Materials*, 5(7):L070801, 2021.
- [39] Arpan Kundu, Yunxiang Song, and Giulia Galli. Influence of nuclear quantum effects on the electronic properties of amorphous carbon. *Proceedings of the National Academy of Sciences*, 119(31):e2203083119, 2022.
- [40] Shan-Tao Lai and Ying-Nan Chiu. Exact computation of the 3-j and 6-j symbols. *Computer physics communications*, 61(3):350–360, 1990.
- [41] Yi-Lun Liao and Tess Smidt. Equiformer: Equivariant graph attention transformer for 3d atomistic graphs. In *International Conference on Learning Representations*, 2023.
- [42] Yi-Lun Liao, Brandon Wood, Abhishek Das, and Tess Smidt. Equiformerv2: Improved equivariant transformer for scaling to higher-degree representations. arxiv preprint arxiv:2306.12059, 2023.
- [43] Yi Liu, Limei Wang, Meng Liu, Yuchao Lin, Xuan Zhang, Bora Oztekin, and Shuiwang Ji. Spherical message passing for 3d molecular graphs. In *International Conference on Learning Representations (ICLR)*, 2022.
- [44] Shengjie Luo, Tianlang Chen, and Aditi S. Krishnapriyan. Enabling efficient equivariant operations in the fourier basis via gaunt tensor products. In *The Twelfth International Conference on Learning Representations*, 2024.
- [45] Leonard C Maximon. 3j, 6j, 9j symbols., 2010.
- [46] Albert Musaelian, Simon Batzner, Anders Johansson, Lixin Sun, Cameron J Owen, Mordechai Kornbluth, and Boris Kozinsky. Learning local equivariant representations for large-scale atomistic dynamics. *Nature Communications*, 14(1):579, 2023.
- [47] Saro Passaro and C Lawrence Zitnick. Reducing so (3) convolutions to so (2) for efficient equivariant gnns. In *International Conference on Machine Learning*, pages 27420–27438. PMLR, 2023.
- [48] Eric Qu and Aditi Krishnapriyan. The importance of being scalable: Improving the speed and accuracy of neural network interatomic potentials across chemical domains. *Advances in Neural Information Processing Systems*, 37:139030–139053, 2024.
- [49] Giulio Racah. Theory of complex spectra. ii. *Physical Review*, 62(9-10):438, 1942.
- [50] Soumya Sanyal, Janakiraman Balachandran, Naganand Yadati, Abhishek Kumar, Padmini Rajagopalan, Suchismita Sanyal, and Partha Talukdar. Mt-cgcnn: Integrating crystal graph convolutional neural network with multitask learning for material property prediction. *arXiv* preprint arXiv:1811.05660, 2018.
- [51] Victor Garcia Satorras, Emiel Hoogeboom, and Max Welling. E (n) equivariant graph neural networks. In *International conference on machine learning*, pages 9323–9332. PMLR, 2021.

- [52] Kristof Schütt, Oliver Unke, and Michael Gastegger. Equivariant message passing for the prediction of tensorial properties and molecular spectra. In *International Conference on Machine Learning*, pages 9377–9388. PMLR, 2021.
- [53] Kristof T Schütt, Huziel E Sauceda, P-J Kindermans, Alexandre Tkatchenko, and K-R Müller. Schnet–a deep learning architecture for molecules and materials. *The Journal of Chemical Physics*, 148(24):241722, 2018.
- [54] Guillem Simeon and Gianni De Fabritiis. Tensornet: Cartesian tensor representations for efficient learning of molecular potentials. Advances in Neural Information Processing Systems, 36, 2024.
- [55] Tess E. Smidt, Mario Geiger, and Benjamin Kurt Miller. Finding symmetry breaking order parameters with euclidean neural networks. *Phys. Rev. Res.*, 3:L012002, Jan 2021.
- [56] Attila Szabo and Neil S Ostlund. *Modern quantum chemistry: introduction to advanced electronic structure theory.* Courier Corporation, 2012.
- [57] Nathaniel Thomas, Tess Smidt, Steven Kearnes, Lusann Yang, Li Li, Kai Kohlhoff, and Patrick Riley. Tensor field networks: Rotation-and translation-equivariant neural networks for 3d point clouds. *arXiv preprint arXiv:1802.08219*, 2018.
- [58] Artur P Toshev, Gianluca Galletti, Johannes Brandstetter, Stefan Adami, and Nikolaus A Adams. E (3) equivariant graph neural networks for particle-based fluid mechanics. *arXiv preprint arXiv:2304.00150*, 2023.
- [59] Richard Tran, Janice Lan, Muhammed Shuaibi, Brandon M Wood, Siddharth Goyal, Abhishek Das, Javier Heras-Domingo, Adeesh Kolluru, Ammar Rizvi, Nima Shoghi, et al. The open catalyst 2022 (oc22) dataset and challenges for oxide electrocatalysts. *ACS Catalysis*, 13(5):3066–3084, 2023.
- [60] Oliver T Unke, Martin Stöhr, Stefan Ganscha, Thomas Unterthiner, Hartmut Maennel, Sergii Kashubin, Daniel Ahlin, Michael Gastegger, Leonardo Medrano Sandonas, Joshua T Berryman, et al. Biomolecular dynamics with machine-learned quantum-mechanical force fields trained on diverse chemical fragments. *Science Advances*, 10(14):eadn4397, 2024.
- [61] DA Varshalovich, AN Moskalev, and VK Khersonskii. Quantum theory of angular momentum. 1987.
- [62] Limei Wang, Yi Liu, Yuchao Lin, Haoran Liu, and Shuiwang Ji. ComENet: Towards complete and efficient message passing for 3d molecular graphs. In Alice H. Oh, Alekh Agarwal, Danielle Belgrave, and Kyunghyun Cho, editors, Advances in Neural Information Processing Systems, 2022.
- [63] Yusong Wang, Shaoning Li, Xinheng He, Mingyu Li, Zun Wang, Nanning Zheng, Bin Shao, Tong Wang, and Tie-Yan Liu. Visnet: a scalable and accurate geometric deep learning potential for molecular dynamics simulation. *arXiv preprint arXiv:2210.16518*, 2022.
- [64] Vesselin Yamakov, Dieter Wolf, Simon R Phillpot, Amiya K Mukherjee, and Herbert Gleiter. Dislocation processes in the deformation of nanocrystalline aluminium by molecular-dynamics simulation. *Nature materials*, 1(1):45–49, 2002.

Appendix Table of Contents

A	Glossary of Notations	16
В	Attention-based Wigner 6j Convolution	17
C	Wigner $3j$ and $6j$ Symbols	17
	C.1 The Wigner 3 <i>j</i> Symbol: Definition and Core Properties	18
	C.2 The Wigner 6j Symbol: Recoupling Coefficients	19
D	Main Theorem Proofs	20
	D.1 Binominal Local Expansion	20
	D.2 Wigner 6 <i>j</i> Recoupling and Node-Based Factorization	23
E	Proof of Equivariance	25
F	Time Complexity	26
G	Additional Lemmas	27
Н	Technical Details Behind E2Former	28
I	Addtional Experiments	30
	I.1 QM9 Results	30
	I.2 Comparison with Equiformer V2	30
J	Hyperparameters	31

A Glossary of Notations

Table 5: Glossary of Notations

Symbol	Description
\mathcal{V}, \mathcal{E}	Set of nodes (vertices) V and edges E in a molecular graph.
$ \mathcal{V} , \mathcal{E} $	Number of nodes and edges in the graph, respectively.
	Often used to denote $ \mathcal{V} $, the number of atoms (nodes).
d	Hidden feature dimension (number of channels) at each spherical degree.
s	Spherical dimension: the number of irreps (from $\ell = 0$ to $\ell = L$).
L, L_{\max}	Maximum angular momentum (highest spherical degree).
$\ell \geq 0, m \in \{-\ell, \dots, \ell\}$	Angular momentum quantum numbers for spherical harmonics.
$L, L_{\text{max}} \\ \ell \geq 0, m \in \{-\ell, \dots, \ell\} \\ \mathcal{R}_m^{(\ell)}(\mathbf{r}) \\ U^{(\ell)}$	Real spherical harmonic of degree ℓ and order m , evaluated at position ${\bf r}$.
$U^{(\ell)}$	An irreducible representation (irrep) of $SO(3)$ at angular momentum ℓ .
$\mathbf{h}_i \in \mathbb{R}^{s imes d}$	Feature representation of node i , containing scalar/vector components up to spherical degree L .
$\mathbf{r}_{ij} \in \mathbb{R}^3$	Relative position vector from node i to node j .
\otimes	Clebsch–Gordan (CG) tensor product of two irreps.
\otimes^{6j}	Wigner 6 <i>j</i> -based tensor product (recoupling) of irreps, reorganizing the CG couplings.
α_{ij}	Attention coefficient between node i and j in an equivariant attention layer.
$C_{\ell_1 m_1, \ell_2 m_2}^{(\ell_3 m_3)}$	Clebsch–Gordan coefficient coupling two irreps ℓ_1,ℓ_2 to an output irreps ℓ_3 .
$C_{ij}^{(\ell_3 m_3)} \\ C_{\ell_1 m_1, \ell_2 m_2}^{(\ell_1 m_1, \ell_2 m_2)} \\ \begin{pmatrix} \ell_1 & \ell_2 & \ell_3 \\ m_1 & m_2 & m_3 \end{pmatrix}$	Wigner $3j$ symbol (equivalently related to Clebsch–Gordan coefficients).
$\begin{cases} j_1 & j_2 & j_3 \\ j_4 & j_5 & j_6 \\ D^{(\ell)}(R) \end{cases}$	Wigner $6j$ symbol, governing recoupling of three angular momenta in different orders.
$D^{(\ell)}(R)$	Wigner D-matrix describing how spherical harmonics of degree ℓ transform under rotation R.
SO(3)	3D rotation group; E2Former is equivariant to transformations in SO(3).
E2Former	The proposed Efficient and Equivariant Transformer architecture.
Wigner 6j Conv	The core convolution module leveraging Wigner 6 <i>j</i> recoupling to shift edge-based operations to nodes.

B Attention-based Wigner 6*i* Convolution

We describe the algorithmic procedure for constructing the Attention-based Wigner 6j Convolution introduced in the main text. Assume that attention coefficients α have been precomputed, either through Query-Key inner products or via MLP-based attention mechanisms such as those in Equiformer v2 [42]. We begin by precomputing the spherical harmonics $\mathcal{R}^{(\ell)}$ up to a maximum degree L based on the input positions \mathbf{r} .

For each degree $k=0,\ldots,L$, we compute an attention-weighted tensor product between the input features **h** and the corresponding spherical harmonics $\mathcal{R}^{(k)}$. This intermediate representation is then modulated by the attention weights α . The resulting tensors are subsequently recoupled using a Wigner 6j tensor product, where each recoupling path is parameterized by the Wigner 6j coefficients—offering a more flexible alternative to the standard Clebsch–Gordan coupling.

Finally, summing over all degrees k yields the output irreducible representations (irreps), which are used to update the node embeddings.

```
Algorithm 1 Wigner 6j-Based Attention
```

```
1: Input: Positions \mathbf{r} \in \mathbb{R}^{N \times 3}, input features \mathbf{h} \in \mathbb{R}^{N \times H \times d \times s}, attention weights \alpha \in \mathbb{R}^{N \times N \times H} (H for number for heads, s for the number for spherical dimension, d for the number of hidden channels), maximum order L
```

```
2: Output: Output features \mathbf{h}_{\text{out}} \in \mathbb{R}^{N \times H \times d \times s}
```

3: Step 1: Precompute Spherical Harmonics

4: for
$$\ell = 0$$
 to L do

5:
$$\mathcal{R}^{(\ell)} \leftarrow \mathrm{SH}(\ell, \mathbf{r})$$

6: end for

7: Step 2: Compute pairwise distances

8:
$$D_{ij} \leftarrow \|\mathbf{r}_i - \mathbf{r}_j\|_2$$

(pairwise Euclidean distance)

9: Step 3: Compute Wigner 6 i tp

10: for k = 0 to L do

11: Compute intermediate tensor product:

$$\mathbf{T}_k \leftarrow \mathtt{clebsch_gorden_tp}(\mathbf{h}, \mathcal{R}^{(k)})$$

12:
$$\alpha_{ijh}^{(k)} \leftarrow \alpha_{ijh}/(D_{ij})^k$$

(entrywise power normalization)

13: Apply attention weights:

$$\mathbf{T}_k \leftarrow \mathtt{einsum}("ijh, jhds \rightarrow \mathrm{ihds"}, \alpha^{(k)}, \mathbf{T}_k)$$

14: Recouple terms using Wigner 6*j* symbols:

$$\mathbf{C}_k \leftarrow \mathtt{Wigner6jTP}(\mathbf{T}_k, \mathcal{R}^{(L-k)})$$

15: Update output: $\mathbf{h}_{\text{out}} \leftarrow \mathbf{h}_{\text{out}} + (-1)^k \binom{L}{k} \mathbf{C}_k$

16: **end for**

Remark B.1. The upshot is that (i) the node-local spherical harmonics $\mathcal{R}^{(u)}(\vec{r}_i)$ can be precomputed once for each node i, and (ii) the partial sum $\sum_j \alpha_{ij}(\mathbf{h}_j \otimes \mathcal{R}^{(\ell-u)}(\vec{r}_j))$ can be treated as a single node-based operation. Thus, the number of tensor products is controlled by $|\mathcal{V}|$ (the number of nodes) rather than $|\mathcal{E}|$ (the number of edges). This is precisely the core reason E2Former achieves improved scalability compared to conventional $\mathrm{SO}(3)$ -equivariant Transformers that do edge-level spherical harmonic products.

C Wigner 3j and 6j Symbols

The Wigner 3j and 6j symbols are fundamental constructs in the representation theory of the Lie group SU(2), intrinsically linked to the theory of angular momentum in quantum mechanics. These symbols emerge as crucial transformation coefficients when decomposing tensor products of irreducible representations of SU(2). They precisely encode the symmetry properties inherent in such decompositions, thereby providing a powerful computational framework for problems involving coupled representations.

C.1 The Wigner 3j Symbol: Definition and Core Properties

The Wigner 3j symbol is denoted by

$$\begin{pmatrix} j_1 & j_2 & j_3 \\ m_1 & m_2 & m_3 \end{pmatrix}, \tag{C.1}$$

where j_i are representation labels (angular momenta) and m_i are their respective components (magnetic quantum numbers). For the symbol to be non-zero, two primary selection rules must be satisfied:

- 1. Conservation of the m quantum number: $m_1 + m_2 + m_3 = 0$.
- 2. Triangle inequalities for the j quantum numbers: $|j_1 j_2| \le j_3 \le j_1 + j_2$, and its cyclic permutations. This ensures that the three angular momenta can form a closed vector triangle.

The explicit algebraic form of the 3j symbol (due to Racah) is given by:

$$\begin{pmatrix}
j_1 & j_2 & j_3 \\
m_1 & m_2 & m_3
\end{pmatrix} = \delta_{m_1 + m_2 + m_3, 0} (-1)^{j_1 - j_2 - m_3} \\
\times \sqrt{\frac{(j_1 + j_2 - j_3)!(j_1 - j_2 + j_3)!(-j_1 + j_2 + j_3)!}{(j_1 + j_2 + j_3 + 1)!}} \\
\times \sqrt{\prod_{k=1}^{3} (j_k + m_k)!(j_k - m_k)!} \\
\times \sum_{z} \frac{(-1)^z}{z!(j_1 + j_2 - j_3 - z)!(j_1 - m_1 - z)!(j_2 + m_2 - z)!} \\
\times \frac{1}{(j_3 - j_2 + m_1 + z)!(j_3 - j_1 - m_2 + z)!},$$
(C.2)

where the summation over the integer z is constrained such that all factorial arguments remain non-negative. The initial δ factor enforces the m-conservation rule.

The 3j symbols possess several important symmetry properties:

- Even permutation of columns leaves the symbol unchanged: $\begin{pmatrix} j_1 & j_2 & j_3 \\ m_1 & m_2 & m_3 \end{pmatrix} = \begin{pmatrix} j_2 & j_3 & j_1 \\ m_2 & m_3 & m_1 \end{pmatrix} = \dots$
- Odd permutation of columns introduces a phase factor $(-1)^{j_1+j_2+j_3}$: $\begin{pmatrix} j_2 & j_1 & j_3 \\ m_2 & m_1 & m_3 \end{pmatrix} = (-1)^{j_1+j_2+j_3} \begin{pmatrix} j_1 & j_2 & j_3 \\ m_1 & m_2 & m_3 \end{pmatrix}$.
- Time-reversal symmetry (negation of all m_i values):

$$\begin{pmatrix} j_1 & j_2 & j_3 \\ -m_1 & -m_2 & -m_3 \end{pmatrix} = (-1)^{j_1+j_2+j_3} \begin{pmatrix} j_1 & j_2 & j_3 \\ m_1 & m_2 & m_3 \end{pmatrix}.$$
 (C.3)

Furthermore, they satisfy crucial orthogonality relations, fundamental for their role as transformation coefficients:

$$\sum_{m_1, m_2} (2j_3 + 1) \begin{pmatrix} j_1 & j_2 & j_3 \\ m_1 & m_2 & m_3 \end{pmatrix} \begin{pmatrix} j_1 & j_2 & j_3' \\ m_1 & m_2 & m_3' \end{pmatrix} = \delta_{j_3, j_3'} \delta_{m_3, m_3'}, \tag{C.4}$$

where the sum is over all allowed m_1, m_2 for fixed j_1, j_2 . Another form is:

$$\sum_{j_2,m_2} (2j_3+1) \begin{pmatrix} j_1 & j_2 & j_3 \\ m_1 & m_2 & m_3 \end{pmatrix} \begin{pmatrix} j_1 & j_2 & j_3 \\ m'_1 & m'_2 & m_3 \end{pmatrix} = \delta_{m_1,m'_1} \delta_{m_2,m'_2}.$$
 (C.5)

C.2 The Wigner 6j Symbol: Recoupling Coefficients

The Wigner 6j symbol, denoted $\{\dots\}$, addresses the recoupling of three angular momenta. It arises when transforming between different sequential coupling schemes for combining three irreducible representations of SU(2). For instance, coupling j_1 and j_2 to an intermediate j_{12} , then coupling j_{12} with j_3 to a final J, versus coupling j_2 and j_3 to j_{23} , then j_1 with j_{23} to J.

It is defined through a sum over products of four 3j symbols:

$$\begin{cases}
j_1 & j_2 & j_3 \\
j_4 & j_5 & j_6
\end{cases} = \sum_{m_1, \dots, m_6} \sum_{m'_1, \dots, m'_3} (-1)^{\sum_{k=1}^6 (j_k - m_k)} \begin{pmatrix} j_1 & j_2 & j_3 \\ m_1 & m_2 & m_3 \end{pmatrix} \begin{pmatrix} j_1 & j_5 & j_6 \\ m'_1 & -m_5 & m_6 \end{pmatrix} \\
\times \begin{pmatrix} j_4 & j_2 & j_6 \\ m_4 & m'_2 & -m'_6 \end{pmatrix} \begin{pmatrix} j_4 & j_5 & j_3 \\ -m'_4 & m'_5 & m'_3 \end{pmatrix},$$
(C.6)

where the m and m' indices are appropriately summed while respecting the 3j symbol selection rules The 6j symbol is directly related to the Racah W-coefficient by a phase factor:

$$\begin{cases}
j_1 & j_2 & j_3 \\
j_4 & j_5 & j_6
\end{cases} = (-1)^{j_1 + j_2 + j_4 + j_5} W(j_1 j_2 j_5 j_4; j_3 j_6).$$
(C.7)

The Racah W-coefficient, W(abcd;ef), is the transformation coefficient between schemes ((a,b)e,d)c and (a,(b,d)f)c. Thus, the 6j symbol effectively captures the algebraic structure of associativity in tensor products of representations.

Symmetries of the 6j symbol are extensive:

- Invariance under any permutation of its columns.
- Invariance under the exchange of upper and lower arguments in any two columns, e.g.: $\begin{cases} j_1 & j_2 & j_3 \\ j_4 & j_5 & j_6 \end{cases} = \begin{cases} j_4 & j_5 & j_3 \\ j_1 & j_2 & j_6 \end{cases}.$

These 24 symmetries reflect the tetrahedral symmetry associated with the symbol, often visualized using Yutsis graphs. Each set $\{j_1, j_2, j_3\}$, $\{j_1, j_5, j_6\}$, $\{j_4, j_2, j_6\}$, and $\{j_4, j_5, j_3\}$ must satisfy the triangle inequalities for the 6j symbol to be non-zero.

An important orthogonality relation (one of several, including the Biedenharn-Elliott identity) is:

$$\sum_{j_3} (2j_3+1)(2j_6+1) \begin{cases} j_1 & j_2 & j_3 \\ j_4 & j_5 & j_6 \end{cases} \begin{cases} j_1 & j_2 & j_3 \\ j_4 & j_5 & j_6' \end{cases} = \delta_{j_6,j_6'} \Delta(j_1,j_5,j_6) \Delta(j_4,j_2,j_6). \quad (C.8)$$

Here, $\Delta(a, b, c) = 1$ if a, b, c satisfy the triangle inequalities, and 0 otherwise.

A remarkable connection to geometry is provided by the Ponzano-Regge asymptotic formula. For large j values, it relates the 6j symbol to the geometry of a tetrahedron whose edge lengths are $j_k + \frac{1}{2}$:

$$\begin{cases} j_1 & j_2 & j_3 \\ j_4 & j_5 & j_6 \end{cases} \approx \frac{1}{\sqrt{12\pi V}} \cos \left(\sum_{k=1}^6 (j_k + \frac{1}{2})\theta_k + \frac{\pi}{4} \right), \tag{C.9}$$

where V is the volume of the tetrahedron and θ_k are the dihedral angles. This formula bridges quantum angular momentum algebra with semi-classical geometric concepts.

D Main Theorem Proofs

D.1 Binominal Local Expansion

Claim D.1 (Multiplicity-One of $V^{(L_{\max})}$ [61, 8]). The irreducible representation $V^{(L_{\max})}$ appears with multiplicity one in the decomposition of $V^{(l_1)} \otimes \cdots \otimes V^{(l_k)}$. That is,

$$V^{(l_1)} \otimes \cdots \otimes V^{(l_k)} \cong \bigoplus_L N_L V^{(L)}, \quad \textit{with } N_{L_{\max}} = 1.$$

Claim D.2 (Schur's Lemma [24]). Let V, W be irreducible representations of a group G over an algebraically closed field. If $T: V \to W$ is a G-equivariant linear map, then either T=0, or $V \cong W$ and T is a scalar multiple of the identity.

Claim D.3 (Recoupling via Wigner 6*j* Symbols [49]). For any two CG coupling trees τ and τ' , the associated contraction operations are related by a unitary transformation:

$$\mathcal{C}_{\tau'} = R_{\tau' \leftarrow \tau} \, \mathcal{C}_{\tau},$$

where $R_{\tau' \leftarrow \tau}$ is a product of Wigner 6j matrices acting on intermediate coupling channels.

Lemma D.4 (Ordering-Invariance of Maximally Coupled Representation). Let $\mathbf{h}_1^{(l_1)}, \ldots, \mathbf{h}_k^{(l_k)} \in V^{(l_1)} \otimes \cdots \otimes V^{(l_k)}$ denote a sequence of irreducible features, where each $V^{(l_i)}$ is the irreducible representation of $\mathrm{SO}(3)$. Let $L_{\mathrm{max}} := \sum_{i=1}^k l_i$. Then for any binary CG coupling tree τ , the projection of the coupled tensor onto the L_{max} subspace,

$$\left[\mathcal{C}_{ au}\left(\mathbf{h}_{1}^{(l_{1})},\ldots,\mathbf{h}_{k}^{(l_{k})}
ight)
ight]^{(L_{ ext{max}})},$$

is invariant to the choice of τ .

Proof. The tensor product $V^{(l_1)} \otimes \cdots \otimes V^{(l_k)}$ admits a decomposition into irreducible components of the form $\bigoplus_L N_L V^{(L)}$, where N_L denotes the multiplicity of the spin-L representation. It is a classical fact (Claim D.1) that the maximal total spin $L_{\max} := \sum_i l_i$ appears with multiplicity one. Consequently, the subspace $V^{(L_{\max})}$ is uniquely defined up to a basis, and any projection onto it is one-dimensional in each magnetic subspace.

Each binary CG coupling tree τ defines a recursive contraction \mathcal{C}_{τ} via successive applications of the Clebsch–Gordan tensor product. For any two such trees τ and τ' , the corresponding coupled features are related by a transformation $\mathcal{C}_{\tau'} = R_{\tau' \leftarrow \tau} \mathcal{C}_{\tau}$, where $R_{\tau' \leftarrow \tau}$ is constructed from a sequence of Wigner 6j symbols. This recoupling matrix is unitary (by Claim D.3) and acts on the space of intermediate angular momentum.

Since $V^{(L_{\text{max}})}$ appears with multiplicity one, Schur's lemma (Claim D.2) implies that any SO(3)-equivariant transformation, such as $R_{\tau'\leftarrow\tau}$, must act as a scalar on this subspace:

$$R_{\tau' \leftarrow \tau}|_{V^{(L_{\max})}} = \lambda_{\tau',\tau} \cdot \mathrm{Id}, \quad \text{with } |\lambda_{\tau',\tau}| = 1.$$

By adopting a fixed phase convention (e.g., the Condon–Shortley convention for CG coefficients), we can choose $\lambda_{\tau',\tau}=1$, yielding

$$\left[\mathcal{C}_{\tau}(\mathbf{h}_1^{(l_1)},\ldots,\mathbf{h}_k^{(l_k)})\right]^{(L_{\max})} = \left[\mathcal{C}_{\tau'}(\mathbf{h}_1^{(l_1)},\ldots,\mathbf{h}_k^{(l_k)})\right]^{(L_{\max})}.$$

An equivalent interpretation is that $V^{(L_{\max})}$ can be realized as the totally symmetric, trace-free subspace of the rank- L_{\max} tensor formed from the inputs $\mathbf{h}_1^{(l_1)},\ldots,\mathbf{h}_k^{(l_k)}$. Since full symmetrization commutes with all permutations and parenthesizations, the final projected tensor is independent of the coupling order. This concludes the proof.

Theorem D.5 (Projection identity for spherical harmonics). Let $\mathbf{r}_{ij} := \mathbf{r}_i - \mathbf{r}_j \in \mathbb{R}^3 \setminus \{\vec{0}\}$ and let $\mathcal{R}^{(l)}(\vec{r})$ denote the degree-l spherical harmonic. For every integer $\ell \geq 0$,

$$\mathcal{R}^{(\ell)}(\mathbf{r}_{ij}) = \left[\left(\mathcal{R}^{(1)}(\mathbf{r}_{ij}) \right)^{\otimes \ell} \right]^{(\ell)},$$

where $(\cdot)^{\otimes \ell}$ is the ℓ -fold tensor product and the $[\cdot]^{(\ell)}$ denotes the orthogonal projector onto the irreducible SO(3) subspace of total angular momentum ℓ .

Proof. The function $\mathcal{R}^{(1)}(\mathbf{r}_{ij})$ transforms according to the irreducible (vector) representation $D^{(1)}$ of SO(3). Hence the tensor power satisfies

$$\left(\mathcal{R}^{(1)}(\mathbf{r}_{ij})\right)^{\otimes \ell} \in \bigotimes^{\ell} D^{(1)} \cong \bigoplus_{l=0}^{\ell} D^{(l)} \otimes \mathbb{C}^{m_l},$$

where m_l is the multiplicity of $D^{(l)}$ in the Clebsch–Gordan decomposition. Applying the projector $[\cdot]^{(\ell)}$ extracts the $D^{(\ell)}$ summand, yielding a rank- ℓ tensor that transforms in the same irrep as $\mathcal{R}^{(\ell)}$.

Because $D^{(\ell)}$ is irreducible, Schur's lemma (Claim D.2) implies that any two non-zero intertwiners from $D^{(\ell)}$ to itself differ by a scalar. Thus the projected tensor must be proportional to the degree- ℓ spherical harmonic:

$$\left[\left(\mathcal{R}^{(1)}(\mathbf{r}_{ij}) \right)^{\otimes \ell} \right]^{(\ell)} = c_{\ell} \, \mathcal{R}^{(\ell)}(\mathbf{r}_{ij}).$$

To determine the constant c_ℓ , evaluate both sides on the north-pole direction $\vec{z}=(0,0,1)$. In the Condon–Shortley convention $\mathcal{R}^{(1)}_{\pm 1}(\vec{z})=0$ and $\mathcal{R}^{(1)}_0(\vec{z})=\sqrt{3/(4\pi)}$, so the only non-vanishing component of the tensor power corresponds to the highest-weight vector $|\ell,\ell\rangle$. A direct Clebsch–Gordan calculation (or induction on ℓ) shows that its norm matches that of $\mathcal{R}^{(\ell)}_\ell(\hat{z})=\sqrt{(2\ell+1)/(4\pi)}$, fixing $c_\ell=1$. Since both sides transform identically under rotations, equality for one direction implies equality for all directions, completing the proof.

Theorem D.6 (Binomial Local Expansion). Let $\vec{r_i}, \vec{r_j} \in \mathbb{R}^3$ denote the positions of two nodes i, j, and let $\vec{r_{ij}} = \vec{r_j} - \vec{r_i}$. For each integer $\ell \geq 1$, let $\mathcal{R}^{(\ell)}(\cdot)$ denote the real-valued spherical harmonics of order ℓ . Then,

$$\mathcal{R}^{(\ell)}(\vec{r}_{ij}) = \left[\left(\mathcal{R}^{(1)}(\vec{r}_{j}) - \mathcal{R}^{(1)}(\vec{r}_{i}) \right)^{\otimes \ell} \right]^{(\ell)} = \sum_{u=0}^{\ell} (-1)^{\ell-u} \binom{\ell}{u} \left[\mathcal{R}^{(u)}(\vec{r}_{j}) \otimes \mathcal{R}^{(\ell-u)}(\vec{r}_{i}) \right]^{(\ell)},$$

where $[\cdot]^{(\ell)}$ denotes projection onto the irreducible subspace of total angular momentum ℓ via Clebsch–Gordan decomposition. Equality holds up to a normalization constant depending on the basis choice for $\mathcal{R}^{(\ell)}$ and the CG convention.

Proof. By Theorem D.5, the spherical harmonic $\mathcal{R}^{(\ell)}(\mathbf{r}_{ij})$ can be constructed by projecting the ℓ -fold tensor product of first-order harmonics onto the irreducible subspace of total angular momentum ℓ :

$$\mathcal{R}^{(\ell)}(\mathbf{r}_{ij}) = \left[\left(\mathcal{R}^{(1)}(\mathbf{r}_j) - \mathcal{R}^{(1)}(\mathbf{r}_i) \right)^{\otimes \ell} \right]^{(\ell)}.$$

This expression follows from the identity $\mathbf{r}_{ij} = \mathbf{r}_j - \mathbf{r}_i$ and the fact that $\mathcal{R}^{(1)}$ is linear in spatial coordinates.

Expanding the tensor power via the multinomial binomial rule yields

$$\left(\mathcal{R}^{(1)}(\mathbf{r}_j) - \mathcal{R}^{(1)}(\mathbf{r}_i)\right)^{\otimes \ell} = \sum_{u=0}^{\ell} (-1)^{\ell-u} \binom{\ell}{u} \sum_{P \in \Pi_u} T_P,$$

where each term T_P corresponds to a specific ordering $P \in \Pi_u$ of the tensor product, containing exactly u factors of $\mathcal{R}^{(1)}(\mathbf{r}_j)$ and $\ell - u$ factors of $\mathcal{R}^{(1)}(\mathbf{r}_i)$. The total number of such orderings is $|\Pi_u| = \binom{\ell}{u}$.

Applying the linear projection operator $[\cdot]^{(\ell)}$ to both sides gives:

$$\left[\left(\mathcal{R}^{(1)}(\mathbf{r}_j) - \mathcal{R}^{(1)}(\mathbf{r}_i) \right)^{\otimes \ell} \right]^{(\ell)} = \sum_{u=0}^{\ell} (-1)^{\ell-u} {\ell \choose u} \sum_{P \in \Pi_u} [T_P]^{(\ell)}.$$

At this point, we invoke the ordering-invariance lemma (Lemma D.4), which states that the projection of a tensor product onto the highest angular momentum subspace (here, ℓ) is invariant under permutation of the tensor factors. Therefore, the projected tensors $[T_P]^{(\ell)}$ are identical for all $P \in \Pi_u$, and depend only on the multiplicities of $\mathcal{R}^{(1)}(\mathbf{r}_i)$ and $\mathcal{R}^{(1)}(\mathbf{r}_i)$ within the product.

We may thus replace the sum over $P \in \Pi_u$ with a multiplicity factor times a single representative term. Letting $T_{\text{rep}} := (\mathcal{R}^{(1)}(\mathbf{r}_j))^{\otimes u} \otimes (\mathcal{R}^{(1)}(\mathbf{r}_i))^{\otimes (\ell-u)}$, we obtain:

$$\sum_{P\in\Pi_u} [T_P]^{(\ell)} = \binom{\ell}{u} \left[T_{\text{rep}}\right]^{(\ell)} = \binom{\ell}{u} \left[(\mathcal{R}^{(1)}(\mathbf{r}_j))^{\otimes u} \otimes (\mathcal{R}^{(1)}(\mathbf{r}_i))^{\otimes (\ell-u)} \right]^{(\ell)}.$$

Finally, note that $(\mathcal{R}^{(1)}(\mathbf{r}))^{\otimes u}$ contains irreducible components of order up to u, and the highest such component is $\mathcal{R}^{(u)}(\mathbf{r})$. Projecting the expression onto total angular momentum ℓ thus yields:

$$\mathcal{R}^{(\ell)}(\mathbf{r}_{ij}) = \sum_{u=0}^{\ell} (-1)^{\ell-u} \binom{\ell}{u} \left[\mathcal{R}^{(u)}(\mathbf{r}_j) \otimes \mathcal{R}^{(\ell-u)}(\mathbf{r}_i) \right]^{(\ell)},$$

which concludes the derivation.

D.2 Wigner 6*j* Recoupling and Node-Based Factorization

Here, we formalize the proof of the Theorem 3.3 for completeness.

Setup: We consider a typical SO(3)-equivariant Transformer layer that performs message passing from each node j in the neighborhood of i using the tensor product $\mathbf{h}_i \otimes \mathcal{R}^{(\ell)}(\vec{r}_{ij})$. Symbolically,

$$\mathbf{h}_i^{\mathrm{new}} = \sum_{j \in \mathcal{N}(i)} \alpha_{ij} (\mathbf{h}_j \otimes \mathcal{R}^{(\ell)}(\vec{r}_{ij})).$$

Goal: To show that the expensive edge-based computation over (i, j) can be reorganized so that the *tensor product* portion (or at least the dominating part of it) depends only on node i and a separate node j portion. This is achieved by:

$$\mathcal{R}^{(\ell)}(\vec{r}_{ij}) \mapsto \sum_{u=0}^{\ell} \left[\mathcal{R}^{(u)}(\vec{r}_i) \right] \otimes^{6j} \left[\mathcal{R}^{(\ell-u)}(\vec{r}_j) \right],$$

together with a rearrangement (via Wigner 6j) of \mathbf{h}_j inside the product.

Theorem D.7 (Node-Based Factorization via Wigner 6*j*). Let $\mathbf{h}_j \in \mathbb{R}^d$ be the feature of node *j*, and let α_{ij} be any scalar weight (e.g. an attention coefficient). In the SO(3)-equivariant layer:

$$\sum_{j \in \mathcal{N}(i)} (\mathbf{h}_j \, \otimes \, \mathcal{R}^{(\ell)}(\vec{r}_{ij})),$$

we can reorganize $\mathcal{R}^{(\ell)}(\vec{r}_{ij})$ into node-i and node-j parts by Theorem D.6 and then apply Wigner 6j recoupling to obtain:

$$\sum_{j \in \mathcal{N}(i)} \left(\mathbf{h}_j \otimes \mathcal{R}^{(\ell)}(\vec{r}_{ij}) \right) = \sum_{u=0}^{\ell} (-1)^{\ell-u} \binom{\ell}{u} \left[\mathcal{R}^{(u)}(\vec{r}_i) \right] \otimes^{6j} \left(\sum_{j \in \mathcal{N}(i)} \left[\mathbf{h}_j \otimes \mathcal{R}^{(\ell-u)}(\vec{r}_j) \right] \right).$$

Proof. We commence with the definition of the SO(3)-equivariant node convolution for node i. Substituting the Binomial Local Expansion for $\mathcal{R}^{(\ell)}(\mathbf{r}_{ij})$ yields:

$$\mathbf{h}_{i} = \sum_{j \in \mathcal{N}(i)} \mathbf{h}_{j} \otimes \left(\sum_{u=0}^{\ell} (-1)^{\ell-u} \binom{\ell}{u} \left[\mathcal{R}^{(u)}(\mathbf{r}_{i}) \otimes \mathcal{R}^{(\ell-u)}(\mathbf{r}_{j}) \right]^{(\ell)} \right). \tag{D.1}$$

Invoking the linearity of the Clebsch-Gordan tensor product \otimes with respect to its second argument, and subsequently interchanging the order of the finite summations (over $j \in \mathcal{N}(i)$ and $u \in [0, \ell]$), Eq. (D.1) is rewritten as:

$$\mathbf{h}_{i} = \sum_{u=0}^{\ell} (-1)^{\ell-u} \binom{\ell}{u} \sum_{j \in \mathcal{N}(i)} \left(\mathbf{h}_{j} \otimes \left[\mathcal{R}^{(u)}(\mathbf{r}_{i}) \otimes \mathcal{R}^{(\ell-u)}(\mathbf{r}_{j}) \right]^{(\ell)} \right). \tag{D.2}$$

We now focus on the term within the summation over j:

$$T_{j,u} = \mathbf{h}_j \otimes \left[\mathcal{R}^{(u)}(\mathbf{r}_i) \otimes \mathcal{R}^{(\ell-u)}(\mathbf{r}_j) \right]^{(\ell)}. \tag{D.3}$$

Let $U_A = \mathbf{h}_j$, $U_C = \mathcal{R}^{(u)}(\mathbf{r}_i)$, and $U_B = \mathcal{R}^{(\ell-u)}(\mathbf{r}_j)$ represent the respective irreducible representations. The term $T_{j,u}$ signifies a specific coupling scheme: U_C (irrep u) and U_B (irrep $\ell-u$) are first coupled, and their product is projected onto the irreducible component transforming as irrep ℓ , denoted $[U_C \otimes U_B]^{(\ell)}$. Subsequently, U_A is coupled with this resulting tensor of irrep ℓ . This scheme corresponds to $(U_A \otimes (U_C \otimes U_B)^{L_{CB} = \ell})$, where $L_{CB} = \ell$ is the fixed intermediate angular momentum.

The theory of angular momentum recoupling, governed by Wigner 6j symbols (as per Definition 2.3), allows for the reordering of tensor product operations while preserving the final irreducible content. We seek to transform $T_{j,u}$ into a form where U_A and U_B are coupled first. Specifically, we apply a

recoupling to achieve the order $U_C \otimes^{6j} (U_A \otimes U_B)$. The transformation from $(U_A \otimes (U_C \otimes U_B)^{L_{CB}=\ell})$ to $(U_C \otimes (U_A \otimes U_B)^{L_{AB}})$ (for any resulting total angular momentum) is a standard result in Wigner-Racah calculus. The operator \otimes^{6j} denotes that the CG tensor product is performed with path weights modified by the appropriate Wigner 6j symbol, which accounts for this change in coupling pathway. Note that the intermediate coupling of $\mathcal{R}^{(u)}(\mathbf{r}_i)$ and $\mathcal{R}^{(\ell-u)}(\mathbf{r}_j)$ results in a constrained irrep ℓ (governed by the projection operator); this gives rise to a constrained Wigner 6j coupling, where the constraint (the intermediate angular momentum being ℓ) is inherently managed by the 6j coefficients encapsulated within the \otimes^{6j} operation. Thus, we can write:

$$\mathbf{h}_{j} \otimes \left[\mathcal{R}^{(u)}(\mathbf{r}_{i}) \otimes \mathcal{R}^{(\ell-u)}(\mathbf{r}_{j}) \right]^{(\ell)} = \mathcal{R}^{(u)}(\mathbf{r}_{i}) \otimes^{6j} \left(\mathbf{h}_{j} \otimes \mathcal{R}^{(\ell-u)}(\mathbf{r}_{j}) \right). \tag{D.4}$$

Substituting Eq. (D.4) into Eq. (D.2):

$$\mathbf{h}_{i} = \sum_{u=0}^{\ell} (-1)^{\ell-u} \binom{\ell}{u} \sum_{j \in \mathcal{N}(i)} \left(\mathcal{R}^{(u)}(\mathbf{r}_{i}) \otimes^{6j} \left(\mathbf{h}_{j} \otimes \mathcal{R}^{(\ell-u)}(\mathbf{r}_{j}) \right) \right). \tag{D.5}$$

The term $\mathcal{R}^{(u)}(\mathbf{r}_i)$ is independent of the summation index j. The operation \otimes^{6j} , like the standard tensor product \otimes , is linear in its second argument with respect to summation. Thus, $\mathcal{R}^{(u)}(\mathbf{r}_i)\otimes^{6j}$ can be factored out of the sum over j:

$$\mathbf{h}_{i} = \sum_{u=0}^{\ell} (-1)^{\ell-u} \binom{\ell}{u} \left(\mathcal{R}^{(u)}(\mathbf{r}_{i}) \otimes^{6j} \left(\sum_{j \in \mathcal{N}(i)} \mathbf{h}_{j} \otimes \mathcal{R}^{(\ell-u)}(\mathbf{r}_{j}) \right) \right). \tag{D.6}$$

This expression is the factorized form of the SO(3)-equivariant node convolution as stated in the theorem.

E Proof of Equivariance

We now formally establish that the Wigner 6j convolution is equivariant under the action of the rotation group SO(3). Define the convolutional output as follows:

$$f(\mathbf{x}) = \sum_{u=0}^{\ell} \left(\mathcal{R}^{(u)}(\mathbf{r}_i) \otimes^{6j} \left(\alpha_{ij} \left(\mathbf{h}_j \otimes \mathcal{R}^{(\ell-u)}(\mathbf{r}_j) \right) \right) \right).$$

We analyze the transformation of this expression under the rotation $R \in SO(3)$. The transformed output is:

$$f(R \cdot \mathbf{x}) = \sum_{u=0}^{\ell} \left(D^{(u)}(R) \mathcal{R}^{(u)}(\mathbf{r}_i) \otimes^{6j} \left(\alpha_{ij} \left(D^{(a)}(R) \mathbf{h}_j \otimes D^{(\ell-u)}(R) \mathcal{R}^{(\ell-u)}(\mathbf{r}_j) \right) \right) \right).$$

Let us define the intermediate quantity:

$$S_u \triangleq \sum_{j \in \mathcal{N}(i)} \alpha_{ij} \, \mathbf{h}_j \otimes \mathcal{R}^{(\ell-u)}(\mathbf{r}_j).$$

Under rotation, this transforms as:

$$\sum_{j \in \mathcal{N}(i)} \alpha_{ij} \left(D^{(a)}(R) \mathbf{h}_j \otimes D^{(\ell-u)}(R) \mathcal{R}^{(\ell-u)}(\mathbf{r}_j) \right) = \left(D^{(a)}(R) \otimes D^{(\ell-u)}(R) \right) S_u.$$

Substituting into the convolution expression yields:

$$f(R \cdot \mathbf{x}) = \sum_{u=0}^{\ell} \left(D^{(u)}(R) \mathcal{R}^{(u)}(\mathbf{r}_i) \otimes^{6j} \left(\left(D^{(a)}(R) \otimes D^{(\ell-u)}(R) \right) S_u \right) \right).$$

Since the Wigner 6j recoupling tensor \otimes^{6j} is SO(3)-equivariant (as the Wigner coefficients are invariant under rotation), we may commute the group action:

$$D^{(u)}(R)\mathcal{R}^{(u)}(\mathbf{r}_i) \otimes^{6j} \left(\left(D^{(a)}(R) \otimes D^{(\ell-u)}(R) \right) S_u \right) = D_{\text{out}}(R) \left(\mathcal{R}^{(u)}(\mathbf{r}_i) \otimes^{6j} S_u \right),$$

where $D_{\text{out}}(R)$ denotes the output representation under SO(3). Therefore:

$$f(R \cdot \mathbf{x}) = \sum_{u=0}^{\ell} D_{\text{out}}(R) \left(\mathcal{R}^{(u)}(\mathbf{r}_i) \otimes^{6j} S_u \right) = D_{\text{out}}(R) f(\mathbf{x}).$$

This completes the proof of SO(3)-equivariance.

F Time Complexity

We analyze the computational complexity of the Wigner-6j convolution, with particular attention to its dependence on the number of nodes \mathcal{V} , the number of channels C, and the maximum angular momentum L. The dominant cost stems from angular momentum coupling via tensor products and Wigner-6j recoupling, while the linear self-mix step introduces an additional quadratic dependence on C. This analysis aligns with the derivations in Appendix C of the eSCN paper for SO(3) convolution.

Let $\mathcal V$ denote the total number of nodes (e.g., atoms), and C the number of channels per irreducible representation. The algorithm involves iterating over all valid angular momentum triplets (L_1,L_2,L_o) up to order L, subject to triangle inequality constraints.

(1) **Tensor Product:** Each tensor product between irreps (L_1, L_2) incurs a cost

$$\Theta(C \cdot L_1 \cdot L_2)$$

(2) Wigner-6j and CG Multiplication: The cost of recoupling the tensor via Wigner-6j coefficients is

$$\Theta(C \cdot L_1 \cdot L_2 \cdot L_o)$$

(3) Summation Step: The final projection onto L_o includes a summation step costing

$$\Theta(C \cdot L_o)$$

per valid triplet.

The summation step is implemented as follows:

The **per-node** complexity of Wigner-6j convolution is therefore:

$$\sum_{L_1=0}^{L} \sum_{L_2=0}^{L} \sum_{L_o=0}^{L} (CL_1L_2 + CL_1L_2L_o + CL_o) = \Theta(CL^6)$$

Linear Self-Mix. After the convolution, a channel-mixing layer (e.g., an MLP) acts independently on each irrep. This operation mixes C channels across each irrep of order L_o , with complexity:

$$\sum_{L_o=0}^{L} \Theta(C^2 L_o) = \Theta(C^2 L^2)$$

Total Complexity. Summing over all nodes V, the total computational complexity is:

$$\Theta(|\mathcal{V}|CL^6 + |\mathcal{V}|C^2L^2)$$

G Additional Lemmas

Lemma G.1 (Many–Body Reduction). *Using Wigner* 6j *convolution, a multi-atomic cluster expansion can be evaluated in* O(|V|) *time instead of* $O(|\mathcal{E}|)$.

Proof. We decompose the MACE architecture into two computational stages and show that each admits nodewise computation at O(|V|) cost.

Stage 1: SO(3)-Equivariant Convolution. The convolutional component of MACE computes, for each node $i \in V$,

$$\mathbf{A}_i := \sum_{j \in \mathcal{N}(i)} \mathbf{h}_j \otimes \mathcal{R}^{(\ell)}(\mathbf{r}_{ij}),$$

which has naive complexity $O(|\mathcal{E}|)$ over all nodes due to edge enumeration.

Stage 2: Self Tensor Product and Projection. The self tensor product $(\mathbf{A}_i)^{\otimes p}$ and projection $[\cdot]^{(L)}$ are purely local operations, independent of neighbors. Since they apply once per node, they require O(|V|) total time.

Key Step: Nodewise Refactorization via Wigner 6*j*. Using Theorem 3.3, we invoke the following identity:

$$\sum_{j\in\mathcal{N}(i)}\mathbf{h}_{j}\otimes\mathcal{R}^{(\ell)}(\mathbf{r}_{ij})=\sum_{u=0}^{\ell}\mathcal{R}^{(u)}(\mathbf{r}_{i})\otimes^{6j}\left(\sum_{j\in\mathcal{N}(i)}\mathbf{h}_{j}\otimes\mathcal{R}^{(\ell-u)}(\mathbf{r}_{j})\right),$$

where \otimes^{6j} denotes a tensor contraction via Wigner 6j recoupling.

Define global moment tensors $\mathbf{M}^{(\ell-u)} := \sum_{j \in V} \mathbf{h}_j \otimes \mathcal{R}^{(\ell-u)}(\mathbf{r}_j)$. These are precomputable in O(|V|) time, and reused across all $i \in V$. The refactorized form becomes

$$\psi_i = \sum_{u=0}^{\ell} \mathcal{R}^{(u)}(\mathbf{r}_i) \otimes^{6j} \mathbf{M}^{(\ell-u)},$$

which is independent of the neighborhood structure and thus computable per node in constant time (for fixed ℓ).

Complexity. The precomputation of $\{\mathbf{M}^{(\ell-u)}\}_{u=0}^{\ell}$ costs O(|V|). The nodewise contractions via \otimes^{6j} are constant-time per node for bounded ℓ , yielding an overall convolutional cost of O(|V|). Since the subsequent self tensor product and projection are already node-local, the total complexity of MACE becomes O(|V|).

H Technical Details Behind E2Former

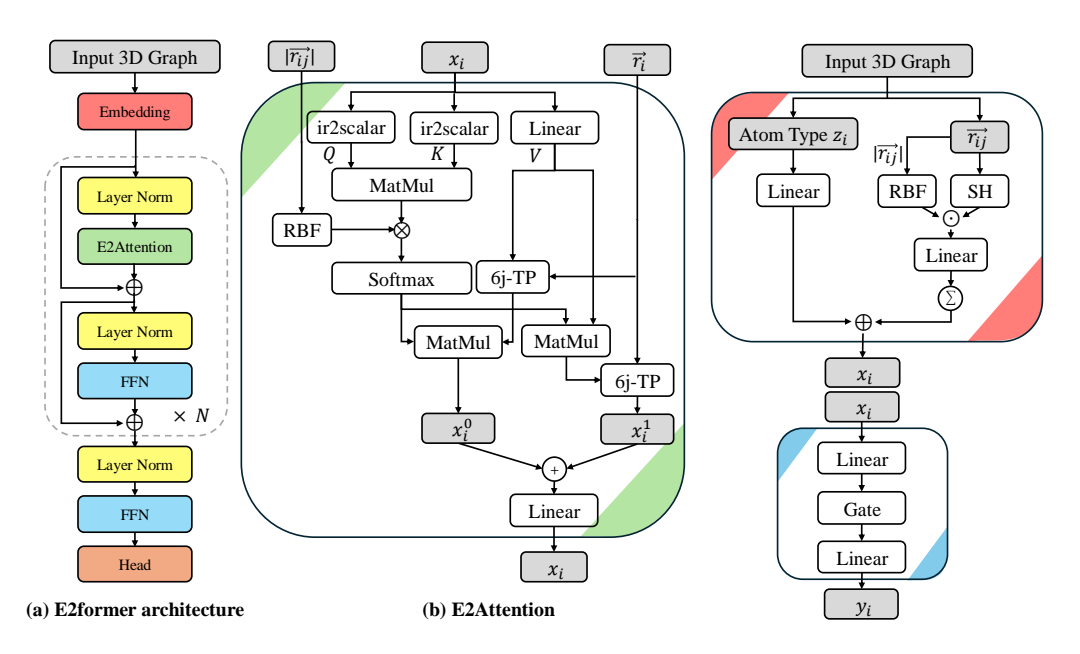


Figure 5: Overview of the E2Former architecture. (a) The main network alternates E2Attention blocks with feedforward layers, repeatedly refining node embeddings from a 3D molecular graph. (b) Within each E2Attention block, scalarized queries/keys (via ir2scalar) are combined with distance-dependent features (RBF) and convolutions (6j-TP), updating the node embeddings equivariantly. (c) The final readout incorporates atomic types and radial/spherical expansions (RBF, SH) into a gated projection that produces the per-atom output y_i .

In our development, we not only want mathematical integrity but also practical usefulness. Thus, E2Former is not solely characterized by Wigner-6j conv, but rather as an architecture that integrates both efficiency and significant engineering components. The benefit of Wigner-6j conv enables us to reallocate the computational budget to increase expressivity elsewhere, such as adding more layers, wider hidden dimensions, or more attention heads.

Architecture Overview. The E2FORMER architecture adheres to the general transformer paradigm, commencing with an embedding layer that generates initial E(3)-equivariant node features. These features are subsequently refined through a stack of E2former blocks, denoted as TransBlock in our implementation. Each TransBlock employs a pre-normalization strategy, structured as: Normalization \rightarrow Transformer Layer \rightarrow Residual Connection \rightarrow Normalization \rightarrow Equivariant Feed-Forward Network (FFN) \rightarrow Residual Connection.

Initial Embedding and Feature Representation. The generation of initial equivariant node features, $\mathbf{h}_i^{(0)}$, for each node i (e.g., an atom) with input coordinates and type, is performed by an Initial Equivariant Embedding module. This module constructs features by aggregating information from the local neighborhood. Interatomic distances are encoded using radial basis functions (RBFs), while relative positions, $\mathbf{r}_j - \mathbf{r}_i$, are represented using spherical harmonics, $\mathcal{R}_m^{(l)}(\vec{p}_j - \vec{p}_i)$, up to a specified maximum degree l_{\max} . The resultant features, $\mathbf{h}_i^{(0)}$, comprise a collection of irreducible representations (irreps) of SO(3). Within each TransBlock, Equivariant Normalization layers are applied before both the attention and FFN sub-layers. These layers operate by normalizing features independently within each irrep channel, which is crucial for stabilizing training and enhancing model performance.

Equivariant Feed-Forward Networks. Subsequent to the attention mechanism, node features are processed by an *Equivariant Feed-Forward Network*. E2FORMER accommodates a variety of FFN

types, configurable via the ffn_type parameter. These include standard equivariant Multi-Layer Perceptrons (MLPs) that operate on spherical harmonic coefficients (e.g., FeedForwardNetwork_s2, FeedForwardNetwork_s3, potentially incorporating grid-based non-linearities inspired by eSCN and EquiformerV2 [47, 42]), as well as explicit many-body interaction modules [6] that integrate equivariant two-body or three-body tensor products. This modular design permits tailored feature processing contingent upon the specific demands of the task.

E2Attention Mechanism. The central component enabling feature interaction in E2FORMER is the *E2Attention* mechanism, which builds upon the Wigner-6*j* Convolution to update node embeddings. A key implementation consideration lies in the treatment of positional information. While many spherical EGNNs normalize relative positions, this practice may discard essential directional cues in Wigner-6*j* Convolution, which is inherently node-centric. To preserve relative geometric information, we retain unnormalized absolute positions in the convolution, and instead apply normalization during the attention coefficient computation.

All-Order Attention Paths. E2Attention explicitly models and adaptively aggregates contributions from multiple *spherical harmonic orders*. Under the $attn_type="all-order"$ configuration, the mechanism includes a zero-order (scalar) path that captures isotropic interactions, a first-order (vector) path using Wigner-6j Convolution configured for order-1 interactions, and higher-order paths (e.g., second-order for l=2) to model more complex anisotropic effects.

Computation of Attention Weights. Attention weights α_{ij} are computed from projected scalar queries and keys derived from \mathbf{h}_i and \mathbf{h}_j , enriched by radial basis function (RBF) embeddings of $\|\mathbf{r}_{ij}\|$ and optionally, learnable embeddings of atomic types z_i, z_j . Geometric information can be incorporated into attention in various ways, such as through the tp_type="dot_alpha" configuration, which directly integrates spherical harmonics into the attention score computation.

Gated Aggregation of Orders. A critical component of E2Attention is the Gated Aggregation of Orders. The contributions from the zero-order $(\mathbf{m}_{ij}^{(0)})$, first-order $(\mathbf{m}_{ij}^{(1)})$, and second-order $(\mathbf{m}_{ij}^{(2)})$ pathways are adaptively combined via a learnable gating mechanism. Specifically, the scalar (l=0) components of the central node's features \mathbf{h}_i are processed through a small MLP to produce gating coefficients $g_i^{(0)}, g_i^{(1)}, g_i^{(2)}$. The aggregated message from neighbor j to node i is given by

$$\mathbf{m}_{ij} = g_i^{(0)} \odot \mathbf{m}_{ij}^{(0)} + g_i^{(1)} \odot \mathbf{m}_{ij}^{(1)} + g_i^{(2)} \odot \mathbf{m}_{ij}^{(2)}$$

The updated node feature \mathbf{h}_i' is then computed by summing the attention-weighted messages from all neighbors:

$$\mathbf{h}_i' = \sum_j \alpha_{ij} \mathbf{m}_{ij}.$$

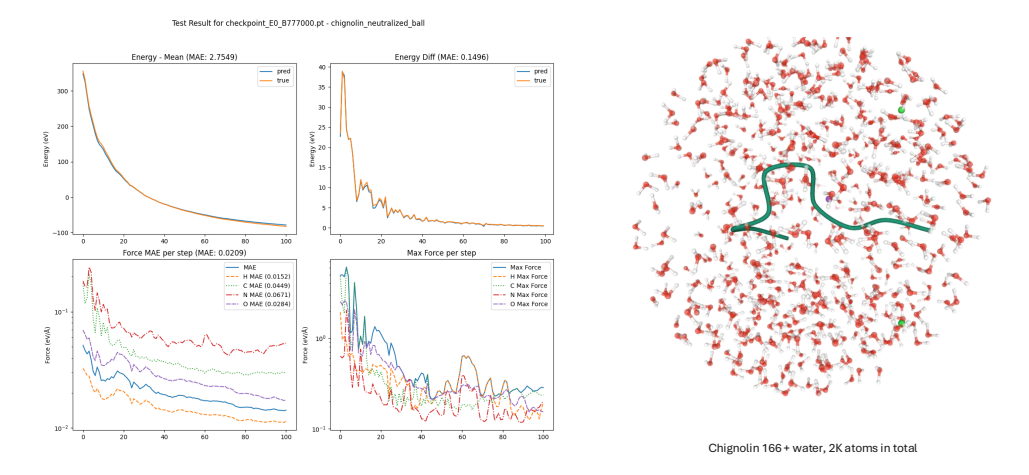


Figure 6: Force MAE on a system of around 2000 atoms, where a chignolin peptide is wrapped with water.

I Addtional Experiments

I.1 QM9 Results

We additionally evaluated our method on the QM9 dataset as a quality check. Due to computational constraints, we report results on three representative energy metrics: U_0 , HOMO, and LUMO. E2Former demonstrates competitive performance compared to Equiformer V2 and its predecessor Equiformer, while GotenNet [2] achieves the best overall results. Nonetheless, we emphasize that our model is primarily designed for larger systems, whereas QM9 represents a relatively small-scale benchmark.

Table 6: Performance on QM9 (U_0 , HOMO, LUMO)

Method	U_0	НОМО	LUMO
E2Former	6.43	14.2	13.6
GotenNet	3.37	13.4	12.2
Equiformer V2	6.17	14.4	13.3
Equiformer	6.59	15.4	14.7

I.2 Comparison with Equiformer V2

To ensure a better comparison with the Equiformer V2 model, we aligned the experimental settings between E2Former and Equiformer V2. Specifically, we adopted identical hyperparameters and architecture configurations for both models, including the number of layers, maximum angular momentum orders, and radial basis functions. This alignment guarantees a controlled comparison and eliminates confounding factors arising from differing model capacities or training settings.

Table 7 summarizes the performance in terms of energy mean absolute error (E), force mean absolute error (F), and inference speed (measured in samples per second). The results indicate that E2Former not only achieves better accuracy on both energy and force predictions but also delivers significantly faster inference speed under matched conditions.

Table 7: Comparison between E2Former and Equiformer V2 under identical hyperparameter settings.

Method	E	F	Number of Layers	$L_{\rm max}$	$M_{\rm max}$	Inference Speed (samples/sec)
E2Former	20.5	270	12	3	2	34
Equiformer V2	23.47	296	12	3	2	22

J Hyperparameters

Table 8: Hyperparameter Configuration for E2Former on OC20, OC22, and SPICE

Hyperparameter	E2Former 33M	E2Former 67M	Description
— General Training Settings —			
optim.lr_initial	0.00015	0.0002	Initial learning rate for the optimizer.
optim.batch_size	128 for OC20/OC22 and 48 for SPICE	64	Training batch size.
— Model Architecture —			
model.backbone.encoder_embed_dim	256	256	Embedding dimension for each node.
model.backbone.hidden_size	256	256	Hidden size for intermediate layers.
model.backbone.num_layers	6	12	Number of E2Former layers.
model.backbone.max_neighbors	20	20	Max neighbors per node for message passing.
model.backbone.irreps_node_embedding	256x0e+256x1e+256x2e+256x3e	256x0e+256x1e+256x2e+256x3e	Irreps for node embeddings up to $\ell = 3$.
model.backbone.irreps_head	16x0e+16x1e+16x2e+16x3e	16x0e+16x1e+16x2e+16x3e	Irreps for the final head up to $\ell = 3$.
model.backbone.attn_scalar_head	16	16	Size of scalar attention head projections.
model.backbone.num_attn_heads	32	32	Number of multi-head attentions per layer.
model.backbone.number_of_basis	256	256	Number of radial basis functions.
model.backbone.max_radius	12 for OC20/22 and 5 for SPICE	12 for OC20/22 and 5 for SPICE	Cutoff radius for local neighborhood.
model.backbone.alpha_drop	0.05	0.05	Drop rate for alpha (e.g., attention dropout).
model.backbone.drop_path_rate	0.05	0.05	Stochastic depth/drop path rate.
model.backbone.basis_type	gaussiansmear	gaussiansmear	Type of radial embedding (Gaussian smearing).
model.backbone.norm_layer	layer_norm_sh	layer_norm_sh	Normalization layer type (LayerNorm in spherical bas
model.backbone.attn_type	all-order	all-order	Attention mechanism covering all spherical orders.
model.backbone.tp_type	dot_alpha	dot_alpha	Type of tensor product (dot + learned scale).
model.backbone.ffn_type	s2	s2	Type of feed-forward network in each block.

NeurIPS Paper Checklist

1. Claims

Question: Do the main claims made in the abstract and introduction accurately reflect the paper's contributions and scope?

Answer: [Yes]

Justification: The claims made in the abstract and introduction directly align with the core contributions: introducing the Wigner 6j convolution, reducing $\mathcal{O}(|\mathcal{E}|)$ complexity to $\mathcal{O}(|\mathcal{V}|)$, and achieving competitive or superior performance on OC20, OC22, and SPICE. See Sec. 1 (Introduction) and Sec. 4 (Results).

Guidelines:

- The answer NA means that the abstract and introduction do not include the claims made in the paper.
- The abstract and/or introduction should clearly state the claims made, including the
 contributions made in the paper and important assumptions and limitations. A No or
 NA answer to this question will not be perceived well by the reviewers.
- The claims made should match theoretical and experimental results, and reflect how much the results can be expected to generalize to other settings.
- It is fine to include aspirational goals as motivation as long as it is clear that these goals
 are not attained by the paper.

2. Limitations

Question: Does the paper discuss the limitations of the work performed by the authors?

Answer: [Yes]

Justification: Limitations, such as the reliance on spherical harmonics and potential inefficiency for very small graphs where edge-level operations dominate, are discussed in Sec. 5. We also acknowledge assumptions of perfect molecular geometries.

Guidelines:

- The answer NA means that the paper has no limitation while the answer No means that the paper has limitations, but those are not discussed in the paper.
- The authors are encouraged to create a separate "Limitations" section in their paper.
- The paper should point out any strong assumptions and how robust the results are to violations of these assumptions (e.g., independence assumptions, noiseless settings, model well-specification, asymptotic approximations only holding locally). The authors should reflect on how these assumptions might be violated in practice and what the implications would be.
- The authors should reflect on the scope of the claims made, e.g., if the approach was only tested on a few datasets or with a few runs. In general, empirical results often depend on implicit assumptions, which should be articulated.
- The authors should reflect on the factors that influence the performance of the approach. For example, a facial recognition algorithm may perform poorly when image resolution is low or images are taken in low lighting. Or a speech-to-text system might not be used reliably to provide closed captions for online lectures because it fails to handle technical jargon.
- The authors should discuss the computational efficiency of the proposed algorithms and how they scale with dataset size.
- If applicable, the authors should discuss possible limitations of their approach to address problems of privacy and fairness.
- While the authors might fear that complete honesty about limitations might be used by reviewers as grounds for rejection, a worse outcome might be that reviewers discover limitations that aren't acknowledged in the paper. The authors should use their best judgment and recognize that individual actions in favor of transparency play an important role in developing norms that preserve the integrity of the community. Reviewers will be specifically instructed to not penalize honesty concerning limitations.

3. Theory assumptions and proofs

Question: For each theoretical result, does the paper provide the full set of assumptions and a complete (and correct) proof?

Answer: [Yes]

Justification: All theoretical claims are accompanied by clearly stated assumptions (e.g., irrep decompositions under SO(3)) and full proofs in Appendix A. Proof sketches are included in the main text (Sec. 3).

Guidelines:

- The answer NA means that the paper does not include theoretical results.
- All the theorems, formulas, and proofs in the paper should be numbered and crossreferenced.
- All assumptions should be clearly stated or referenced in the statement of any theorems.
- The proofs can either appear in the main paper or the supplemental material, but if they appear in the supplemental material, the authors are encouraged to provide a short proof sketch to provide intuition.
- Inversely, any informal proof provided in the core of the paper should be complemented by formal proofs provided in appendix or supplemental material.
- Theorems and Lemmas that the proof relies upon should be properly referenced.

4. Experimental result reproducibility

Question: Does the paper fully disclose all the information needed to reproduce the main experimental results of the paper to the extent that it affects the main claims and/or conclusions of the paper (regardless of whether the code and data are provided or not)?

Answer: [Yes]

Justification: We detail all training protocols, datasets, and evaluation metrics in Sec. 4 and Appendix B. Full experimental setup is sufficient to reproduce key results.

Guidelines:

- The answer NA means that the paper does not include experiments.
- If the paper includes experiments, a No answer to this question will not be perceived well by the reviewers: Making the paper reproducible is important, regardless of whether the code and data are provided or not.
- If the contribution is a dataset and/or model, the authors should describe the steps taken to make their results reproducible or verifiable.
- Depending on the contribution, reproducibility can be accomplished in various ways. For example, if the contribution is a novel architecture, describing the architecture fully might suffice, or if the contribution is a specific model and empirical evaluation, it may be necessary to either make it possible for others to replicate the model with the same dataset, or provide access to the model. In general, releasing code and data is often one good way to accomplish this, but reproducibility can also be provided via detailed instructions for how to replicate the results, access to a hosted model (e.g., in the case of a large language model), releasing of a model checkpoint, or other means that are appropriate to the research performed.
- While NeurIPS does not require releasing code, the conference does require all submissions to provide some reasonable avenue for reproducibility, which may depend on the nature of the contribution. For example
- (a) If the contribution is primarily a new algorithm, the paper should make it clear how to reproduce that algorithm.
- (b) If the contribution is primarily a new model architecture, the paper should describe the architecture clearly and fully.
- (c) If the contribution is a new model (e.g., a large language model), then there should either be a way to access this model for reproducing the results or a way to reproduce the model (e.g., with an open-source dataset or instructions for how to construct the dataset).
- (d) We recognize that reproducibility may be tricky in some cases, in which case authors are welcome to describe the particular way they provide for reproducibility. In the case of closed-source models, it may be that access to the model is limited in

some way (e.g., to registered users), but it should be possible for other researchers to have some path to reproducing or verifying the results.

5. Open access to data and code

Question: Does the paper provide open access to the data and code, with sufficient instructions to faithfully reproduce the main experimental results, as described in supplemental material?

Answer: [Yes]

Justification: We provide anonymized links in the supplemental material to the code repository and data preprocessing scripts. Upon acceptance, we will release these publicly under MIT license.

Guidelines:

- The answer NA means that paper does not include experiments requiring code.
- Please see the NeurIPS code and data submission guidelines (https://nips.cc/public/guides/CodeSubmissionPolicy) for more details.
- While we encourage the release of code and data, we understand that this might not be possible, so "No" is an acceptable answer. Papers cannot be rejected simply for not including code, unless this is central to the contribution (e.g., for a new open-source benchmark).
- The instructions should contain the exact command and environment needed to run to reproduce the results. See the NeurIPS code and data submission guidelines (https://nips.cc/public/guides/CodeSubmissionPolicy) for more details.
- The authors should provide instructions on data access and preparation, including how to access the raw data, preprocessed data, intermediate data, and generated data, etc.
- The authors should provide scripts to reproduce all experimental results for the new proposed method and baselines. If only a subset of experiments are reproducible, they should state which ones are omitted from the script and why.
- At submission time, to preserve anonymity, the authors should release anonymized versions (if applicable).
- Providing as much information as possible in supplemental material (appended to the paper) is recommended, but including URLs to data and code is permitted.

6. Experimental setting/details

Question: Does the paper specify all the training and test details (e.g., data splits, hyperparameters, how they were chosen, type of optimizer, etc.) necessary to understand the results?

Answer: [Yes]

Justification: Data splits, optimizer (AdamW), hyperparameter selection, and training epochs are all included in Appendix B and Table 2.

Guidelines:

- The answer NA means that the paper does not include experiments.
- The experimental setting should be presented in the core of the paper to a level of detail that is necessary to appreciate the results and make sense of them.
- The full details can be provided either with the code, in appendix, or as supplemental
 material.

7. Experiment statistical significance

Question: Does the paper report error bars suitably and correctly defined or other appropriate information about the statistical significance of the experiments?

Answer: [No]

Justification: This follows the community standards.

Guidelines:

• The answer NA means that the paper does not include experiments.

- The authors should answer "Yes" if the results are accompanied by error bars, confidence intervals, or statistical significance tests, at least for the experiments that support the main claims of the paper.
- The factors of variability that the error bars are capturing should be clearly stated (for example, train/test split, initialization, random drawing of some parameter, or overall run with given experimental conditions).
- The method for calculating the error bars should be explained (closed form formula, call to a library function, bootstrap, etc.)
- The assumptions made should be given (e.g., Normally distributed errors).
- It should be clear whether the error bar is the standard deviation or the standard error
 of the mean.
- It is OK to report 1-sigma error bars, but one should state it. The authors should preferably report a 2-sigma error bar than state that they have a 96% CI, if the hypothesis of Normality of errors is not verified.
- For asymmetric distributions, the authors should be careful not to show in tables or figures symmetric error bars that would yield results that are out of range (e.g. negative error rates).
- If error bars are reported in tables or plots, The authors should explain in the text how they were calculated and reference the corresponding figures or tables in the text.

8. Experiments compute resources

Question: For each experiment, does the paper provide sufficient information on the computer resources (type of compute workers, memory, time of execution) needed to reproduce the experiments?

Answer: [Yes]

Justification: We report GPU type (A100 40GB), average runtime per epoch, and total compute usage per benchmark task (Appendix C).

Guidelines:

- The answer NA means that the paper does not include experiments.
- The paper should indicate the type of compute workers CPU or GPU, internal cluster, or cloud provider, including relevant memory and storage.
- The paper should provide the amount of compute required for each of the individual experimental runs as well as estimate the total compute.
- The paper should disclose whether the full research project required more compute than the experiments reported in the paper (e.g., preliminary or failed experiments that didn't make it into the paper).

9. Code of ethics

Question: Does the research conducted in the paper conform, in every respect, with the NeurIPS Code of Ethics https://neurips.cc/public/EthicsGuidelines?

Answer: [Yes]

Justification: The study complies with the NeurIPS Code of Ethics. No sensitive data or personally identifiable information is used.

Guidelines:

- The answer NA means that the authors have not reviewed the NeurIPS Code of Ethics.
- If the authors answer No, they should explain the special circumstances that require a deviation from the Code of Ethics.
- The authors should make sure to preserve anonymity (e.g., if there is a special consideration due to laws or regulations in their jurisdiction).

10. Broader impacts

Question: Does the paper discuss both potential positive societal impacts and negative societal impacts of the work performed?

Answer: [Yes]

Justification: We discuss societal benefits in molecular simulation and drug design in Introduction.

Guidelines:

- The answer NA means that there is no societal impact of the work performed.
- If the authors answer NA or No, they should explain why their work has no societal impact or why the paper does not address societal impact.
- Examples of negative societal impacts include potential malicious or unintended uses (e.g., disinformation, generating fake profiles, surveillance), fairness considerations (e.g., deployment of technologies that could make decisions that unfairly impact specific groups), privacy considerations, and security considerations.
- The conference expects that many papers will be foundational research and not tied to particular applications, let alone deployments. However, if there is a direct path to any negative applications, the authors should point it out. For example, it is legitimate to point out that an improvement in the quality of generative models could be used to generate deepfakes for disinformation. On the other hand, it is not needed to point out that a generic algorithm for optimizing neural networks could enable people to train models that generate Deepfakes faster.
- The authors should consider possible harms that could arise when the technology is being used as intended and functioning correctly, harms that could arise when the technology is being used as intended but gives incorrect results, and harms following from (intentional or unintentional) misuse of the technology.
- If there are negative societal impacts, the authors could also discuss possible mitigation strategies (e.g., gated release of models, providing defenses in addition to attacks, mechanisms for monitoring misuse, mechanisms to monitor how a system learns from feedback over time, improving the efficiency and accessibility of ML).

11. Safeguards

Question: Does the paper describe safeguards that have been put in place for responsible release of data or models that have a high risk for misuse (e.g., pretrained language models, image generators, or scraped datasets)?

Answer: [NA]

Justification: Our released models and datasets are low-risk and not subject to misuse concerns. No generative models or scraped data are involved.

Guidelines:

- The answer NA means that the paper poses no such risks.
- Released models that have a high risk for misuse or dual-use should be released with necessary safeguards to allow for controlled use of the model, for example by requiring that users adhere to usage guidelines or restrictions to access the model or implementing safety filters.
- Datasets that have been scraped from the Internet could pose safety risks. The authors should describe how they avoided releasing unsafe images.
- We recognize that providing effective safeguards is challenging, and many papers do not require this, but we encourage authors to take this into account and make a best faith effort.

12. Licenses for existing assets

Ouestion: Are the creators or original owners of assets (e.g., code, data, models), used in the paper, properly credited and are the license and terms of use explicitly mentioned and properly respected?

Answer: [Yes]

Guidelines:

Justification: We use OC20, OC22, and SPICE datasets, each cited with license information.

- The answer NA means that the paper does not use existing assets.
- The authors should cite the original paper that produced the code package or dataset.

- The authors should state which version of the asset is used and, if possible, include a URL.
- The name of the license (e.g., CC-BY 4.0) should be included for each asset.
- For scraped data from a particular source (e.g., website), the copyright and terms of service of that source should be provided.
- If assets are released, the license, copyright information, and terms of use in the package should be provided. For popular datasets, paperswithcode.com/datasets has curated licenses for some datasets. Their licensing guide can help determine the license of a dataset.
- For existing datasets that are re-packaged, both the original license and the license of the derived asset (if it has changed) should be provided.
- If this information is not available online, the authors are encouraged to reach out to the asset's creators.

13. New assets

Question: Are new assets introduced in the paper well documented and is the documentation provided alongside the assets?

Answer: [NA]

Justification: No new datasets or pretrained models are released. Only architectural code and training recipes are shared.

Guidelines:

- The answer NA means that the paper does not release new assets.
- Researchers should communicate the details of the dataset/code/model as part of their submissions via structured templates. This includes details about training, license, limitations, etc.
- The paper should discuss whether and how consent was obtained from people whose asset is used.
- At submission time, remember to anonymize your assets (if applicable). You can either create an anonymized URL or include an anonymized zip file.

14. Crowdsourcing and research with human subjects

Question: For crowdsourcing experiments and research with human subjects, does the paper include the full text of instructions given to participants and screenshots, if applicable, as well as details about compensation (if any)?

Answer: [NA]

Justification: The paper does not involve human participants or crowdsourcing tasks.

Guidelines:

- The answer NA means that the paper does not involve crowdsourcing nor research with human subjects.
- Including this information in the supplemental material is fine, but if the main contribution of the paper involves human subjects, then as much detail as possible should be included in the main paper.
- According to the NeurIPS Code of Ethics, workers involved in data collection, curation, or other labor should be paid at least the minimum wage in the country of the data collector.

15. Institutional review board (IRB) approvals or equivalent for research with human subjects

Question: Does the paper describe potential risks incurred by study participants, whether such risks were disclosed to the subjects, and whether Institutional Review Board (IRB) approvals (or an equivalent approval/review based on the requirements of your country or institution) were obtained?

Answer: [NA]

Justification: No research involving human subjects is conducted.

Guidelines:

- The answer NA means that the paper does not involve crowdsourcing nor research with human subjects.
- Depending on the country in which research is conducted, IRB approval (or equivalent) may be required for any human subjects research. If you obtained IRB approval, you should clearly state this in the paper.
- We recognize that the procedures for this may vary significantly between institutions and locations, and we expect authors to adhere to the NeurIPS Code of Ethics and the guidelines for their institution.
- For initial submissions, do not include any information that would break anonymity (if applicable), such as the institution conducting the review.

16. Declaration of LLM usage

Question: Does the paper describe the usage of LLMs if it is an important, original, or non-standard component of the core methods in this research? Note that if the LLM is used only for writing, editing, or formatting purposes and does not impact the core methodology, scientific rigorousness, or originality of the research, declaration is not required.

Answer: [No]

Justification: LLMs were not used in the development of methods or experimental results. Editing assistance may have been used, but not for scientific reasoning or generation.

Guidelines:

- The answer NA means that the core method development in this research does not involve LLMs as any important, original, or non-standard components.
- Please refer to our LLM policy (https://neurips.cc/Conferences/2025/LLM) for what should or should not be described.